SPECIAL COMMUNICATION

The SHERLOC Calibration Target on the Mars 2020 Perseverance Rover: Design, Operations, Outreach, and Future Human Exploration Functions

Marc D. Fries · Carina Lee · Rohit Bhartia · Joseph Razzell Hollis · Luther W. Beegle · Kyle Uckert et al. [full author details at the end of the article]

Abstract

The Scanning Habitable Environments with Raman and Luminescence for Organics and Chemicals (SHERLOC) is a robotic arm-mounted instrument onboard NASA's *Perseverance* rover. SHERLOC combines imaging via two cameras with both Raman and fluorescence spectroscopy to investigate geological materials at the rover's Jezero crater field site. SHERLOC requires *in situ* calibration to monitor the health and performance of the instrument. These calibration data are critically important to ensure the veracity of data interpretation, especially considering the extreme martian environmental conditions where the instrument operates. The SHERLOC Calibration Target (SCT) is located at the front of the rover and is exposed to the same atmospheric conditions as the instrument. The SCT includes 10 individual targets designed to meet all instrument calibration requirements. An additional calibration target is mounted inside the instrument's dust cover. The targets include polymers, rock, synthetic material, and optical pattern targets. Their primary function is calibration of parameters within the SHERLOC instrument so that the data can be interpreted correctly. The SCT was also designed to take advantage of opportunities for supplemental science investigations and includes targets intended for public engagement. The exposure of materials to martian atmospheric conditions allows for opportunistic science on extravehicular suit (i.e., "spacesuit") materials. These samples will be used in an extended study to produce direct measurements of the expected service lifetimes of these materials on the martian surface, thus helping NASA facilitate human exploration of the planet. Other targets include a martian meteorite and the first geocache target to reside on another planet, both of which increase the outreach and potential of the mission to foster interest in, and enthusiasm for, planetary exploration. During the first 200 sols (martian days) of operation on Mars, the SCT has been analyzed three times and has proven to be vital in the calibration of the instrument and in assisting the SHERLOC team with interpretation of *in situ* data.

Keywords Mars instruments · Raman and fluorescence spectroscopy · Calibration

1 Introduction

On 18 February 2021, the Mars 2020 *Perseverance* rover successfully landed in Jezero crater, Mars, with four primary mission objectives: 1) Explore the record of an ancient martian environment in order to understand its geological history and assess its past habitability, 2) Identify areas with high biosignature preservation potential and detect any potential biosignatures, 3) Collect a suite of scientifically-compelling samples for potential shipment to Earth by a future mission, and 4) Collect data and perform experiments to prepare for human exploration of Mars (Farley et al. 2020). The Scanning Habitable Environments with Raman and Luminescence for Organics and Chemicals (SHERLOC) instrument is an arm-mounted deep-ultraviolet (deep-UV or DUV) fluorescence and Raman spectrometer that, in combination with the rest of the *Perseverance* payload, enables these goals through sub-millimeter-scale, spatially-resolved detection and characterization of organic matter and minerals on surface targets (Bhartia et al. 2021). As detailed in Bhartia et al. (2021), SHERLOC consists of three detection subsystems, the DUV fluorescence and Raman spectrometer and two cameras: the Autofocus Context Imager (ACI) and the Wide Angle Topographic Sensor for Operations and eNgineering (WATSON). The instrument heads for all three subsystems are housed together in the SHERLOC Turret Assembly (STA), a package mounted on the turret at the end of *Perseverance's* robotic arm (RA).

1.1 SHERLOC Spectroscopy

SHERLOC generates Raman and fluorescence maps that provide organic and mineralogical data within spatial context. For spectroscopy, a pulsed NeCu hollow cathode laser, with an emission at 248.579 nm, illuminates the target over a ∼110-micron diameter laser spot. SHERLOC utilizes an internal fine-motion steering scanner mirror to raster the laser over a 7×7 mm field of view. Raman scattering and fluorescence emission from the target are collected and are separated using a single diffraction grating and detected using a single DUV-sensitive charge-coupled-detector (CCD). The spectrometer has a spectral range from 250-360 nm with an average spectral resolution of 0.296 nm (~ 40 cm^{-1}). Due to the presence on the CCD of a Rayleigh scattered plasma emission line at 252.659 nm and a secondary laser line at 252.930 nm, the usable Raman region spans ∼800 to 4000 cm^{-1}. The spectral resolution was chosen to enable the characterization of several astrobiologically-relevant organics and minerals, including C–H, C–N, C=O, and C=C functional groups, carbonates, perchlorates, sulfates and phyllosilicates (Beegle et al. 2015; Bhartia et al. 2021; Uckert et al. 2021; Razzell Hollis et al. 2021a). With DUV excitation, fluorescence emission collected in the 275 to 360 nm region, is spectrally offset from the Raman region (253-275 nm) such that the weaker Raman features are not obscured by fluorescence interference. To enable a compact design (352 mm $\times$ 176 mm $\times$ 276 mm), and to project a high spectral resolution Raman spectrum and a low spectral resolution fluorescence spectrum on a single CCD, the spectrometer design uses an off-axis parabolic grating and aspherical and spherical mirrors. This results in collected light projected across the detector in a non-traditional, curved fashion (a "spectral smile"; Bhartia et al. 2021).

1.2 SHERLOC Imaging

The ACI and spectrometer are co-boresighted, while WATSON is not. RA and turret movements are commanded to position either the ACI and spectrometer, or WATSON, to observe a given target. While the ACI and spectrometer can view the same target with one RA positioning, the arm and/or turret must be moved to allow WATSON to view that same target.

The ACI is used to focus the spectrometer laser and document the texture and structure of observed rock and regolith targets. It produces grayscale images over a 500-600 nm bandpass to provide context images with a 10.1 μm/pixel spatial resolution. In addition to the high-resolution co-located imaging provided by the ACI, WATSON is a red-green-blue (RGB) color camera with a macro lens that can image targets over a range of working distances (measured from lens to target) to provide pictures of geological materials and hardware at a range of spatial scales (Bhartia et al. 2021), including self-portraits of the rover. Like its Mars Science Laboratory (MSL) Mars Hand Lens Imager (MAHLI) predecessor, typical WATSON imaging on Mars is performed at working distances of ∼2.9 cm to ∼35 cm, providing images ranging from ∼17 to ∼132 μm/pixel (Yingst et al. 2016). With its ability to focus at infinity, WATSON is also fully capable of imaging targets at greater distances. SHERLOC spectral maps can be positioned within ACI images for context, and ACI images can likewise be nested within lower spatial resolution WATSON images; WATSON color can also be applied to "colorize" ACI images (Wogsland et al. 2022).

1.3 SHERLOC Calibration

The combined context images and spectral maps enable a spatial understanding of organics, minerals, and chemicals allowing for the detection of potential morphological biosignatures at sub-millimeter scales. To achieve SHERLOC science goals, several parameters need to be measured on the instrument including peak position, correlations between spectral maps and images, instrument spectrometer alignment, and spectral throughput, before overall instrument performance can be assessed. Proper spectral calibration requires a segmented polynomial fit to calibrate the spectrometer wavelength (Uckert et al. 2021), which is routinely refined and updated through measurements of the SHERLOC calibration target (SCT) as well as a calibration target placed on the interior of the instrument dust cover.

The collection of calibration data is critically important to ensure the veracity and interpretation of data obtained from SHERLOC measurements. SHERLOC operates on the arm and—while the instrument was designed to maintain alignment and performance in the martian environment—the daily thermal cycles, aeolian dust, and percussion/drilling operations require periodic assessment of alignment, calibration, and performance of the instrument to obtain the most accurate data being measured. The calibration targets employed on spaceflight instruments serve a vital function ensuring instrument performance can be assessed, as needed, over the course of the mission, as instruments experience degraded abilities due to routine aging (e.g., Barnes et al. 2011; Campbell et al. 2014; Helbert et al. 2014; Manrique et al. 2020; Kinch et al. 2020; Lopez-Reyes et al. 2020; Yingst et al. 2020). Calibration targets also have a rich history of supplementary use for ancillary science functions and education and public outreach. SHERLOC's calibration targets expand on the traditions of past missions in all respects. For one, the targets include fabric and polymer materials used by NASA to construct extravehicular suits (i.e., "spacesuits"). These samples will be used in an extended study to produce direct measurements of the expected service lifetimes of these materials on the martian surface, thus helping facilitate future human exploration of the planet. Other targets include a martian meteorite and the first geocaching target to reside on another planet, both of which increase the public outreach potential of the mission to foster interest in and enthusiasm for planetary exploration.

The SCT, which refers to the entire calibration assembly, is attached near the RA shoulder azimuth actuator, in front of the rover (Fig. 1). It consists of ten individual targets mounted into an assembly: two different aluminum gallium nitride (AlGaN) targets which generate spectral features at 264 and 340 nm, a diffuse transmission target, a piece of the SaU 008
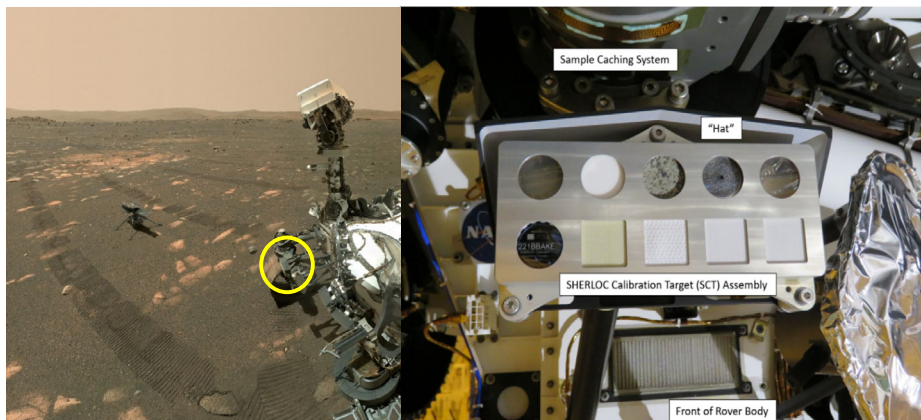
Fig. 1 Left panel shows the location of the SHERLOC Calibration Target (SCT) identified by the yellow circle in the rover self-portrait obtained by WATSON on Sol 46; each rover wheel track is about 40 cm wide. Right panel is a photograph of the SCT attached to the Perseverance rover at the NASA/California Institute of Technology Jet Propulsion Laboratory (JPL) with cover plate removed for final inspection. (L-R, top): AlGaN (Raman), diffuse transmission target, Sayh al Uhaymir 008 (SaU 008) meteorite, intensity maze, AlGaN (fluorescence). (L-R, bottom): Polycarbonate (spacesuit visor material) over geocache coin, spacesuit fabrics Vectran, Ortho-Fabric, Teflon, and nGimat coated Teflon; circle targets have a 20 mm diameter

martian meteorite, a chrome-printed target, an optically transparent polycarbonate target printed with optical imagery, and four different spacesuit polymer materials (Vectran, Ortho-Fabric, Teflon, and nGimat coated Teflon). Each target, plus an 11th target mounted inside the ACI/spectrometer opaque dust cover, was designed to enable SHERLOC to meet specific mission-level requirements, as well as to support future human mission to Mars. This paper describes the SCT's development and requirements and reports the initial measurements of the SCT by SHERLOC on Earth and on Mars. Use of the SCT, and other rover hardware, for in-flight (on Mars, post-landing) WATSON instrument characterization was described by Edgett (2021).

2 SCT Design, Assembly, and Testing

2.1 Calibration Parameters

The SCT was designed to monitor eleven SHERLOC parameters that were used to develop requirements that went into the design of the instrument (Table 1). These requirements can be broken into three separate types of calibrations for the deep UV laser, the ACI imager, and the fluorescence/Raman spectrometer. To minimize the number of targets necessary for calibration, a SHERLOC laboratory analog instrument was used to develop the requirements and the target specifications.

The NeCu deep UV hollow cathode pulsed laser has an electron transition at 248.579 nm and will not spectrally change over time or temperature. However, to achieve the science goals for detection and classification of organics, the laser needs to illuminate the target with an energy density that is defined, in part, by the number of laser pulses used to acquire a single spectrum. While a direct quantitative measure of energy/pulse is ideal, a relative measure of energy/pulse over the age of the laser is sufficient. Since the laser energy will

Table 1 Relations between mission requirements (columns at left) and individual SCT targets (rows at top). Target columns highlighted in grey were present in the original design but descoped to satisfy a redesign prior to Critical Design Review (CDR). A single requirement (*R8*) is fulfilled external to the SCT using color calibration targets on the Mastcam-Z calibration target (Kinch et al. 2020). Note that all requirements are satisfied by the final suite of 11 targets (right hand column). Some targets satisfy multiple requirements, providing a measure of design redundancy

Req. #	Description	Martian Meteorite	Ambient light diffuser	Intensity standard	UV Mirror	AlGaN on Sapphire (264 nm)	AlGaN on Sapphire (340 nm)	Polycarbonate and Geocache	Ortho-Fabric	nGimat coated Teflon	Vectran	Dacron	Teflon	Mastcam-Z color targets	Targets satisfying requirement (excepting removed targets)
Target: Supplier:		Natural History Museum of London	Opsira GmbH	Applied Image Inc.	Teledyne Acton Optics	Texas Tech U.	Texas Tech U.	NASA JSC/EC5 and Applied Image Inc.	NASA JSC/EC5	NASA JSC/EC5	NASA JSC/EC5	NASA JSC/EC5	NASA JSC/EC5	Mastcam-Z	
R1	Calibrate autofocus for Raman spectroscopy function				X	X	X	X	X	X	X	X	X		9
R2	Calibrate Raman spectral accuracy							X	X	X	X	X	X		6
R3	Calibrate fluorescence spectral accuracy							X	X	X	X	X	X		6
R4	Quantify Raman instrument response to analyte			X											1
R5	Collect image of laser spot for focus and laser health					X	X								2
R6	Calibrate autofocus function for imaging cameras							X							1
R7	Perform ambient light reflection measurement		X												1
R8	Calibrate color response of the WATSON camera													X	1
R9	Perform spatial resolution calibration for imaging cameras			X				X							2
R10	Perform spatial calibration for Raman+fluorescence mapping	X													1
R11	Prepare for human exploration of Mars by including EVA materials							X	X	X	X	X	X		6

change with use, it is considered a consumable and requires that the number of pulses be counted (Hein et al. 2022). As the laser pulses, Ne is consumed, lost by trapping of sputtered Cu atoms. To enable testing prior to the prime Mars mission, the laser was filled above the optimum fill pressure (12 torr of Ne). This allowed for SHERLOC operations through the pre-launch/launch and post-landing checkout, reaching an optimum during the prime mission, followed by a slow degradation. The internal calibration target and an internal photodiode are used to monitor the laser energy before and after each analysis and provides a means to adjust the number of laser pulses required to optimize laser lifetime. However, to assess energy density, this measurement requires augmentation with analysis of external calibration targets.

The laser spot size needs to be monitored as the instrument experiences mechanical stresses that can change optical alignments. SHERLOC is attached to the turret through the rotary percussive drill via six vibration isolators. The instrument undergoes diurnal temperature fluctuations of over 80° C each martian day (or sol, equivalent to 1.027 Earth days). There are 24 different optical elements and a scanning mirror which move the laser spot over a surface. 15 of these optical elements have the potential to change the laser spot size/shape and thus affect the overall spectral response and instrument performance. Monitoring laser spot size permits tracking for potential changes and alerts the SHERLOC team to adjust operations parameters accordingly.

The SHERLOC spectrometer consists of fixed optics which were demonstrated to be highly athermal as well as maintain alignment through a low temperature vibration test used to simulate drilling and abrading on Mars. However, dust, vibration from drilling and diurnal stress requires that the spectrometer alignment, throughput, and overall performance are periodically assessed. In addition, assessment of the CCD for hot/cold pixels, dark performance over temperature, or damage from radiation, are needed to optimize performance.

The ACI is used to focus the spectrometer within arm placement accuracies in the z-direction (from surface to front of cover lens). It also allows for co-location of the laser spot within images for direct observations of surface textures and correlation to mineralogy. Monitoring the focus position of the ACI relative to the spectrometer is critical to understanding spectroscopic results. Additional assessment of the laser/spectrometer/imager boresight ensures knowledge of the location of the spectroscopic analyses.

2.2 Design & Fabrication

The SCT was designed, assembled, and tested at NASA Johnson Space Center's (JSC) Astromaterials Research and Exploration Science (ARES) division and Jacobs Engineering, Inc. (Graff et al. 2019). Fabrication of the SCT was performed by Jacobs Engineering, Inc., in a NASA JSC cleanroom rated for ISO 7 ($< 325,000$ particles, >0.5 micron/m^3, and 60 HEPA air filter changes per hour) level of airborne particulate control. All components were encapsulated until assembly, which was performed on a laminar flow bench. A total of four SCT models were made: an engineering model (EM), a flight model (FM), a flight spare (FS), and a curation model (CM). All four were fabricated, cleaned, and conditioned using the same procedure (Sect. 2.4).

The initial concept design of the SCT was first rendered in computer-assisted drawings (CAD) in 2016 with continuing revision through the development cycle. The target is 150 $\times$ 89 $\times$ 33 mm in size with a mass of 437 grams (Fig. 2). The hardware consists primarily of aluminum, stainless steel, and titanium. The SCT had to be designed to allow for arm placement accuracies of $\sim$1 cm, meaning that while the arm attempts to place the instrument optics at dead center on a given SCT target, this positioning can be off as much as a 1 cm. This constraint defined the size of the calibration target.
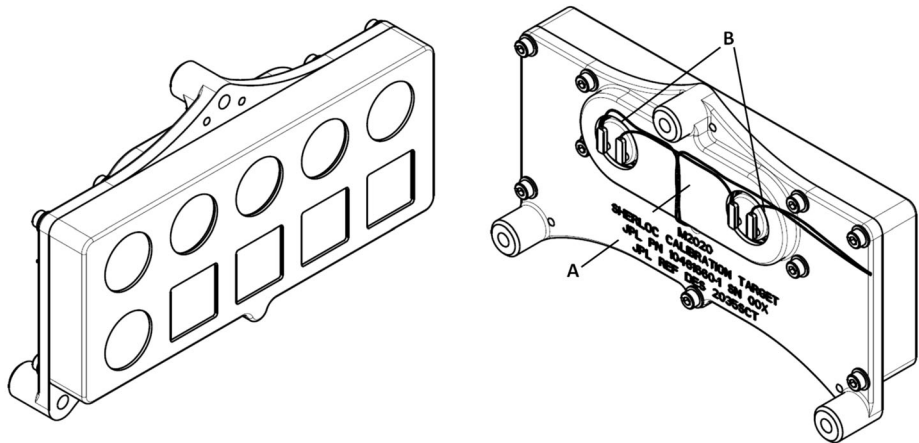
Fig. 2 CAD diagram oblique view of the front (left) and rear (right) of the SCT. View on the right shows the location of the A) cruise decontamination heater, below the cover plate, and B) two thermostats. These were on at all times during cruise, except during eclipse, when they had to be turned off due to limited power

The SCT was designed to be mounted at the front of the rover on its arm bracket, allowing the SHERLOC Turret Assembly access to each target unhindered. The notional location of the SCT attachment moved to several places on the rover as part of the resource balancing which occurs during payload development. The final location resulted in a downsizing of the SCT area from the initial 12 notional targets to 10 due to the field of view of the hazard cameras (hazcams). The SCT development team found a solution that descoped two targets and redesigned two others, producing a smaller target suite while still meeting all calibration requirements (Table 1). A mirror for imaging the laser spot was removed as it was thought that the aluminum faceplate could provide autofocus determination. Additionally, it was determined that a redesign of what is now called the maze target would enable determination of both laser throughput and laser spot size. A spacesuit material target consisting of Dacron was removed after consultation with the spacesuit office at NASA JSC. It was thought that while all the spacesuit materials exhibit nominal off-gassing that are within acceptable limits, Dacron had the least desirable off-gassing qualities amongst the spacesuit materials and could contribute to contamination of other spacecraft surfaces during interplanetary cruise. During this period, several other changes were also made from initial proposed targets. The diffuse ambient target was retained but modified to be single color rather than a previous plan for red, green, and blue (RGB) targets for WATSON calibration. The color targets were removed as it was determined that the requirement for WATSON color response can be satisfied using color targets on the Mastcam-Z calibration target (Kinch et al. 2020).

Four of the SCT targets perform double duty as both calibrants for spectroscopy and as outreach facilitators. The guiding principle for inclusion of outreach-oriented targets is that each target was required to satisfy one of the SHERLOC calibration requirements but could also incorporate features or functions intended to generate public interest. The four targets that serve this dual function, described in detail below, are the geocache coin target, the SaU 008 martian meteorite, the spacesuit materials, and the intensity maze target.

The SCT has ten individual target locations, with six accommodating 25 mm round (20 mm exposed) hard targets of various thickness, and four 20 × 20 mm square openings which expose a portion of spacesuit material retained by a soft goods sub-assembly. A small thermal sub-assembly is included that allows for heating of three targets to reduce

contamination risk during interplanetary cruise. All of the target materials were placed in the SCT without epoxy or other adhesives, as these materials fluoresce and could lead to potential contamination of the target surfaces. All targets and sub-assemblies were pressure-fitted into the SCT housing with a compressed wave spring mount to provide compression from behind. When attached to the rover, the SCT included a "Remove Before Flight" cover plate which protected the targets from contamination during Assembly, Testing, and Launch Operations (ATLO).

2.3 Description of Calibration Target Materials

The SCT has ten individual targets consisting of different materials for instrument calibration. Each target is described in detail below.

2.3.1 AlGaN Targets (2) for Raman (264 nm) and Fluorescence (340 nm)

Each of the two AlGaN targets is a coating of aluminum gallium nitride (AlGaN) on a sapphire disk. AlGaN 264 calibrates the wavelength of the Raman region and the AlGaN 340 calibrates the wavelength of the fluorescence region (Uckert et al. 2021). The 264 nm and 340 nm AlGaN targets were provided by Texas Tech University (Lubbock, Texas, USA) and satisfy the mission requirements for Raman (R2, Table 1) and fluorescence (R3, Table 1) spectral accuracy, respectively. The AlGaN standards produce a photoluminescence band that is broad but has a stable peak wavenumber over a wide range of operating conditions.

2.3.2 Diffuse Transmission Target

The diffuse transmission (DT) target, a commercially purchased piece of Diffusil-UV, is an opaque, fused silica glass containing a homogeneous, unordered distribution of gas bubbles of ∼3 microns in size. DT was manufactured by Opsira GmbH (Weingarten, Germany). DT is used for ambient light calibration, diffuse white balance, and fused silica Raman spectral signature. The gas bubbles equally scatter light in all directions, making the diffuser an almost perfect Lambertian scatterer. The fused silica substrate is transparent to deep UV light, allowing for the Lambertian scattering of light throughout the entire SHERLOC spectral range. It satisfies the mission requirement for ambient light reflection and is one of the three targets on the SCT that was heated for decontamination during the cruise period of its flight to Mars.

2.3.3 Intensity Maze Target

The intensity maze target consists of chrome on silica glass (Fig. 3a). The chrome coating and the uncoated silica parts of the maze are each 200 μm thick. At optimum focus, the laser is focused to a ∼110 μm spot size. The intensity of the signal can be monitored when the laser scans over the chrome and silica regions of the maze target. Using a pre-programmed line scan, the maze pattern ensures that the laser will hit both the silica and chrome regions of the target during a scan. This occurs independent of the arm placement accuracy with respect to distance from and angle to the target as well as rotation of the turret. Calibration of the laser spot size and intensity, the response of the spectrometer CCD, and pointing accuracy of the scanning mirror, can all occur without needing ground-in-the-loop activities. Measurement of the beam size is used in the calculation of the total laser energy deposited at the surface and is used to provide geologic context for each spectrum, relative to features visible in the corresponding ACI and WATSON images.

Fig. 3 Images of the three primary public outreach targets: **a**) the intensity maze target, **b**) the geocache coin and **c**) the SaU 008 martian meteorite. Of note in **b**) the checkerboard tiles are 0.025 × 0.025 mm and the dancing man figures consist of 100 micron-wide lines

2.3.4 Geocache Coin and Polycarbonate Target

The geocache coin (Fig. 3b) is a custom product purchased from Applied Imaging, Inc. (Rochester, NY, USA). It sits behind a polycarbonate disk cut from material used to manufacture spacesuit helmet visors; the polycarbonate coupon was provided from NASA JSC's Life Support Systems stock. As a calibration material for WATSON and ACI imaging, the geocache coin monitors camera spatial resolution performance as a function of focus position. The top portion of the coin contains a graphic consisting of line pairs ranging from 4 line pairs per mm to 114 line pairs per mm. This microscopic optical resolution test, derived from the 1951 US Air Force Resolution Test MIL-STD-150A standard, will enable the assessment of spatial resolution across a range of motion for WATSON and ACI. The graphical representation in the top left, and the Dancing Men Cypher, additionally allow for assessment of resolution without requiring ground-in-the-loop RA repositioning of the cameras. The stick figures in the Dancing Men Cypher are 100 microns in width and act as a *de facto* Air Force Resolution Target if arm placement uncertainties place the instrument very low on that target.

The geocache coin is also used for education and public outreach (EPO) and includes two codes intended to engage members of the international geocaching community. Geocaching is a recreational activity that is commonly termed as a global treasure hunt, whereby "cache owners" hide containers (geocaches) that include a logbook. The owners post the coordinates of those containers online for others to find and log (e.g., Cameron 2017). Geocaching is commonly used as a platform for STEM (science, technology, engineering, and mathematics) engagement with the public. For example, the Geological Society of America has a joint program with Geocaching Headquarters (HQ) (Seattle, WA, USA) called "Earthcaches" where people note the coordinates of geologically-relevant places and the geocacher must go to those places and answer questions about the geology to get credit for the geocache (e.g., Zecha and Hilger 2015; Zecha and Regelous 2018). There has even been a geocache on the International Space Station (ISS). Standard geocaches are in fixed locations and must be logged in person, so only one astronaut (Rick Mastracchio) was ever able to find the geocache on the ISS (Schudiske 2013). Despite the general public not being able to find the cache in person, the first log of the ISS cache was celebrated in November 2013 by 1,100 events held around the world by the geocaching community. The ISS trackable was the first ever off-planet trackable and it demonstrated that geocaching trackables could be a productive format to engage the public in space science (e.g., Schlatter and Hurd 2005; O'Hara 2008; Matherson et al. 2008; Gram-Hansen 2009).

There are many facets to geocaching, and one aspect that enables the average geocacher to actively participate is the "trackables" concept. Trackables are different from standard geocaches as they are items with unique identifying codes that can be moved around either from cache to cache or carried and logged once someone finds the unique code. In addition to the geocache that went to the ISS, several "Travel Bugs" (i.e., a specific type of geocaching trackable) also went to the ISS, and were returned to Earth starting in 2008. Since that time, one of them has received 5980 logs, with each log representing a different person that has physically engaged with the trackable.

The SHERLOC team reached out to Geocaching HQ to gauge their interest in having the first-ever interplanetary trackable on the SCT on the *Perseverance* rover. Instead of a "Travel Bug", we decided to embed the code on a silicate disk mounted behind the transparent polycarbonate target as a "trackable" cache. Geocaching HQ chose the code 221BBaker as a nod to the address from the Sherlock Holmes novels to stay on theme with the SHERLOC and WATSON instruments. We also included a "Dancing Men Cypher" (Doyle 1903) below the trackable code that, when decrypted, gives a message which adds additional intrigue and increases public engagement as geocaches are commonly riddled with such puzzles.

The geocaching community was made aware that a trackable was going to Mars, and that participants should monitor the images being downlinked and placed on the internet in raw form by NASA/Caltech-JPL to find the code to log the first interplanetary trackable. The log page for the trackable remained locked until WATSON sent the first images back of the SCT that were clear enough to see the code. On 17 March 2021, the image was released and the trackable page (Internet Resource 1) was unlocked. The watchlist had over 10,000 people on it and a torrent of logs followed. As of 14 February 2022, there have been over 79,000 individual logs of the trackable calibration target from geocachers worldwide.

2.3.5 Martian Meteorite

The Sayh al Uhaymir 008 (SaU 008) martian (shergottite) meteorite was found in Oman in 1999 (Internet Resource 2) and a sample was provided for the SCT through an extended loan from the Natural History Museum (NHM) of London (Fig. 3c). SaU 008 satisfies calibration requirement R10 (Table 1) for spatial calibration of Raman/fluorescence mapping, as its well-characterized mineralogy and rock texture allows alignment of images and a quantitative measure of Raman and fluorescence response of a host of Mars-relevant minerals. It also provides considerable scientific return and outreach through public engagement. More importantly, the target serves a pivotal role for interpretation of data collected during the Mars surface mission by facilitating direct comparison with the large body of data collected in laboratories on Earth. In addition to their inorganic components, which includes minerals that can be detected by SHERLOC, martian meteorites have been shown to contain an inventory of abiotically-produced organic refractory/macromolecular carbon (Steele et al. 2012, 2016, 2018, 2022). The primary mineralogy of these meteorites is igneous and the reaction pathways forming organic material have been linked to impact generation, electrochemical reduction of CO_2 via secondary aqueous processing, serpentinization, and carbonation reactions. Thus, this makes these meteorites ideal as a calibration standard for the SHERLOC flight instrument and to establish an abiotic background signal to enable possible biosignature differentiation with what is measured in the martian rocks by *Perseverance* (Steele et al. 2016). This allows several conjoined tasks to be fulfilled: 1) verification of mineralogy and correct functioning of the instrument, 2) Raman and fluorescence spectral calibration, 3) understanding of instrument and rover cleanliness and contamination, and 4) degradation of martian materials during the course of the mission.

Several martian meteorites were examined as options and SaU 008 was chosen on the basis of its relatively large available mass, physical toughness, and coarse grain structure. As a high-mass martian meteorite, SaU 008 still has sufficient mass available for scientific use on Earth for a wide variety of analyses with an extensive range of instrumental techniques. Also, because this calibration target contains native martian carbon, it would be possible for SHERLOC to characterize its response to the martian surface environment and provide a direct measure of degradation of native martian carbon species during surface exposure. The relative physical toughness of SaU 008 was deemed necessary to survive the acceleration and vibrational loading inherent in launch and landing, and indeed the meteorite endured vibration and shock testing without visible change (Sect. 3.2, Fig. 13c). SaU 008 features a relatively coarse-grained texture for a martian meteorite, which simplifies SHERLOC imaging during rover operations. The outreach potential of this target is also far-reaching, as samples cut during preparation of the SCT target will allow for direct public interaction at the NHM in London with sibling samples of the same rock that is now on Mars.

The processing of the SaU 008 sample took place in the Meteorite Thin Section Laboratory at NASA JSC. The sample was first cut on a Buehler Isomet saw, fitted with a diamond blade, in order to prepare a slab piece from which two target wafers would be cut. A bath of 190 proof ethyl alcohol was used for cooling and cuttings removal. The bath tray was lined with cleaned aluminum foil in order to save the cuttings after the ethyl alcohol had evaporated. The slab was to be cored with a diamond-edged coring bit mounted to a mini milling machine, but after one attempt it was determined that the machine would damage the sample beyond use. An alternate plan was conceived to use the Isomet saw to make cuts to the slab that resulted in a rough cylinder from which the sample wafers could be sawn. The cylinder was then mounted on a Well Diamond 3032 wire saw equipped with a 200 micron cutting wire. The sample proved to be too hard and coarsely-grained for the fine cutting wire to make a straight cut; the wire broke several times during this attempt. Consequently, the decision was made to use the Isomet saw with a thinner blade. The rough cylinder was successfully cut into four pieces; the two innermost wafers were selected for further shaping. The remaining splits, including collected fines, were assigned split numbers, weighed, and returned to NHM.

The two wafers were shaped on a Buehler Ecomet lapping wheel fitted with 3M silicon carbide abrasive discs. After the wafer edges were lapped to the required diameter, they were scribed with marks to denote which flat face of the wafer was the innermost surface. This surface was to be the exposed face, once mounted in the SCT fixture, and thus was left undisturbed as much as possible. This surface was gently hand lapped to ensure an optically flat face that is devoid of saw marks. The opposite face was carefully lapped and measured with an outside micrometer until the entire wafer was consistently 3 mm in thickness. The finished wafers were ultrasonically cleaned in a bath of 200 proof ethyl alcohol. All of the SaU 008 samples, packing materials, and containers were handled only with nitrile gloves or lab-cleaned stainless-steel tools.

Due to the uniqueness of this sample, the EM and CM models substituted an Earth-derived basalt in place of the martian meteorite in order to test the fidelity of those models.

2.3.6 Extravehicular Suit ("Spacesuit") Materials

The spacesuit materials have well-known Raman spectra that can be used for wavelength calibration. This is the first-time spacesuit materials have been sent to Mars. They were chosen in order to support future landed human activities on the surface of Mars; an understanding of how the martian radiation environment affects the properties of spacesuit materials
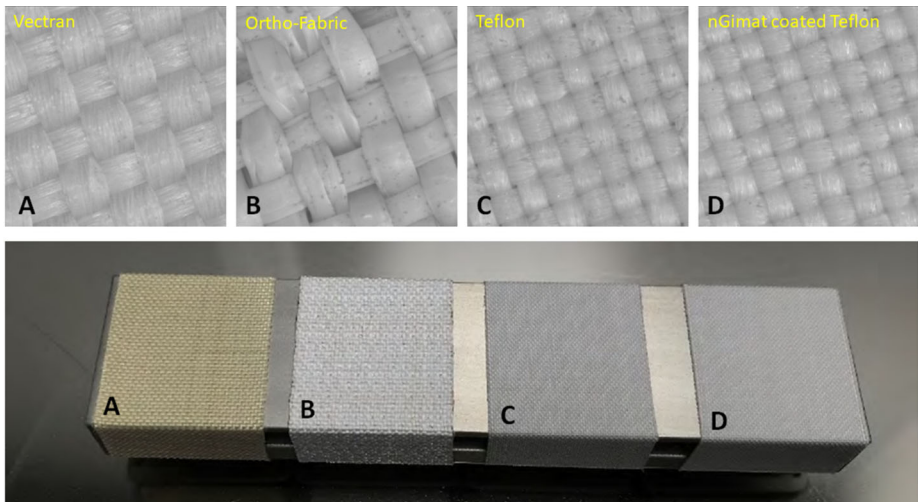
Fig. 4 Top: Sol 59 ACI sub-frames (256 by 256 pixels) of spacesuit materials **a**) Vectran, **b**) Ortho-Fabric, **c**) Teflon, and **d**) nGimat coated Teflon; each image covers an area 2.59 mm wide. Bottom: spacesuit materials in preparation for integration onto the SCT at NASA JSC curation laboratory; metal softgoods mounting bar is 107 mm in length with 23 mm wide softgood strips

is critical for the success of human-based martian missions and for the safety of future astronauts. The Advanced Spacesuit team at NASA JSC selected and initially tested spacesuit materials in order to understand the effects of UV radiation in a simulated Mars environment (Larson and Fries 2017). The study measured the mass, tensile strength, and chemical composition of nine materials prior to and post UV radiation. These results helped the team to choose appropriate spacesuit materials for inclusion on the SCT (Fig. 4). The "softgoods" (i.e., typically non-durable textile products) materials that were ultimately chosen for the SCT were Vectran, Ortho-Fabric, Teflon, and a technology demonstration material, nGimat coated Teflon. The primary purpose of all softgoods targets is to function as a human exploration target (satisfies mission requirement R11, Table 1) and secondarily to calibrate Raman (R2) and fluorescence (R3) spectral accuracy. This is the first-time spacesuit materials have been sent to Mars. Each material, including the polycarbonate helmet visor material (which is mounted in front of the geocache target described above), is explained in detail below.

Polycarbonate The polycarbonate (Makrolon UC with SDC MP-101 hard coat) material that overlays the geocache coin is a piece of extravehicular mobility unit (EMU) helmet visor. It satisfies the three mission requirements as a human exploration target (R11), Raman and fluorescence spectral accuracy (R2, R3), and EPO. The samples used on the SCT are directly cut out of the EMU stock material, which was manufactured and supplied by Air-Lock, Inc. (located in Milford, CT, USA).

Vectran The Vectran fabric (Fig. 4a) is used on the palm of spacesuit gloves, as it has high tensile strength that helps to protect against cuts. Vectran has been used as a material for all airbag landings on Mars. The Vectran material for the SCT was sourced from the JSC's Spacesuit and Crew Survival Systems collection.

Ortho-Fabric Ortho-Fabric (Fig. 4b) is a blend of Nomex/Teflon/Kevlar ripstop woven fabric and it is the primary material that makes up the outermost layer of the spacesuit. It is

a Thermal Micrometeoroid Garment (TMG) component and was therefore intended to provide thermal and micrometeoroid impact protection. The Ortho-Fabric material for the SCT was sourced from the JSC's Spacesuit and Crew Survival Systems collection.

Teflon A Teflon fabric (Fig. 4c) comprises the outer layer of the spacesuit glove, back of hand, and gauntlet. The material is slick so it resists snags and tears and it provides an abrasion-resistant layer for the suit. The Teflon material for the SCT was sourced from the JSC's Spacesuit and Crew Survival Systems collection.

nGimat-Coated Teflon The nGimat-coated Teflon (Fig. 4d) is a product technology demonstration. The superhydrophobic coating, developed by Engi-Mat (located in Lexington, KY, USA), was designed as a dust-resistant coating that may provide a level of self-cleaning performance. nGimat-coated Teflon is being considered as a TMG material. nGimat-coated Teflon for the SCT was sourced from JSC's Spacesuit and Crew Survival Systems collection in collaboration with Engi-Mat.

These materials provide a unique opportunity to study the degradation behavior of spacesuit material in a Mars surface environment. The material samples will be exposed to martian atmosphere, surface radiation, aeolian dust, and thermal cycling for years while being periodically analyzed by SHERLOC in order to determine material stability, compositional changes, and any signs of degradation. The *in situ* SHERLOC analyses will serve as a ground-truth for the laboratory studies to enable at least limited comparisons between the material degradation on Mars and under simulated martian conditions on Earth as well as inform the suit design and material selection of future Mars-specific spacesuits to be used in human exploration of the planet. A companion laboratory study is in preparation to directly measure the service lifetimes of spacesuit materials by subjecting a large suite of identical materials to analogous conditions in a Mars environmental chamber, calibrating their response against the SCT materials, and then directly measuring physical and mechanical properties. This multi-year study will produce high-fidelity measurements for the expected service lifetimes of spacesuits long before any astronaut sets foot on Mars. Other products of this study will include the first Mars environment chamber calibrated using degradation behavior of materials placed on Mars, which can then be used to study other materials, components, and assemblies.

2.4 Contamination Control

The SCT pre-clean and final-clean procedures were documented in the SCT process procedures report. The cleaning process is derived from a combination of the following documents: JSC-29742 Cleaning Genesis Sample Return Canister for Flight: Lessons for Planetary Sample Return, DPI 5001-04 Rev. G Hardware Cleaning; JSC Engineering Directorate; Manufacturing Enterprise, and JPL D-95514, JPL Mars 2020 Project Contamination Control Implementation Plan (Allton et al. 2002; Worthy 2020; JPL D-95514).

Briefly, the pre-clean procedure involves gently scrubbing SCT parts in 95% ultrapure water (UPW) and 5% Brulin 815 GD detergent/degreaser at ambient temperature, heated (52 °C) UPW rinse, heated (52 °C) ultrasonication in UPW/Brulin, and a final UPW rinse at ambient temperature. The final-clean procedure involves UPW cascade tank (70 °C), UPW rinse at ambient temperature, visual particle counts, $N_{2(g)}$ and oven (<110 °C) dry, triple bag package (1-FEP Teflon, 2-Nylon, 3-Nylon), and final transfer to the JSC Genesis Laboratory for ultra-cleaning. The ultra-cleaning stage involved a rinse in 99.9% HPLC-grade isopropanol (IPA), and a cycle of UPW/Brulin and UPW rinse and sonication under ambient

or heated conditions, according to a procedure derived from the abovementioned contamination control documents. All hard and softgoods targets delivered by the vendor were visually inspected, rinsed in 99.9% IPA, sonicated in an IPA bath, rinsed with IPA, and dried with curation grade $N_{2(g)}$. Additional details on the composition of our UPW and curation grade $N_{2(g)}$ are provided in McCubbin et al. (2019).

In order to avoid the deposition of carbon and other contaminants within the clean room at JSC, a "Remove Before Flight" cover was left on the SCT until right before the radioisotope thermoelectric generator (RTG) power source on the rover was integrated. During launch and interplanetary cruise, the rover was inside an aero-shell that, while vented, did have the potential to contribute contamination via hardware outgassing. In order to limit the amount of contamination build-up on some of the targets, they were heated to $+30$ to $+40°$ C and monitored using an embedded thermostat (Fig. 2). Two heaters were placed behind the DT and maze targets, with SaU 008 placed between them. This was determined to be the best location during thermal modeling of the calibration target to reduce contamination across the entire target with the two allocated heaters.

2.5 Attachment to Rover Body

After assembly, only the FM and FS underwent flight testing, while the CM was assembled without electronic and thermal components and was placed into long-term curation at JSC. The FS endured three shock tests, functional tests, photographic documentation, and inspection before final preparation. The FM endured vibration and function testing as well as imaging and inspection before final preparation and delivery to JPL/Caltech. For the final preparation, analysis, and verification, the FM calibration target was put through a thermal vacuum (TVAC) test and both the FM and FS were baked out according to contamination control procedures (Sect. 2.4) at JPL. After an instrument analysis and surface analysis and verification, the FS was placed on standby under $N_{2(g)}$ purge, while the FM was integrated with the *Perseverance* rover.

The SCT was integrated with the *Perseverance* rover on 16 August 2019 in a cleanroom rated for ISO 8 particulate control in the ATLO facility at JPL. An anomaly was identified on 3 December 2019 wherein Brayco 815Z, a fluorinated aliphatic lubricant used to lubricate the "elbow" joint of the rover's RA, had leaked several drops onto the SCT assembly. This required the FS calibration target to be fully qualified to replace the contaminated FM. The FM and FS are identical with the exception that the martian meteorite target differs slightly in mineralogical texture. The FS model passed the vibration test and was inspected, imaged, and delivered to JPL for further testing and integration with the rover. The "Remove Before Flight" cover plate was taken from the CM target and delivered with the FS as a potential replacement. An "umbrella"—a protective hat made from an aluminum alloy—was added between the RA elbow tripod and the calibration target as a secondary mitigation for the elbow leak and to prevent future contamination (Fig. 1). The umbrella was tested and verified prior to integration. On 12 March 2020, the original FM SCT removed from the rover and replaced by the FS SCT.

Launch occurred on 30 July 2020 from pad LC41 at Cape Canaveral Air Force Station (now Space Force Station), Florida, and the rover landed in Jezero crater, Mars, on 18 February 2021 after a 203-day flight. SHERLOC collected its first WATSON images of the SCT on 16 March 2021 (Sol 26) (Fig. 5).

2.6 Calibration During Operations

Before and after every SHERLOC measurement, a spectrum of a 277 nm AlGaN target, mounted on the inside of the dust cover, is collected as a single-point calibration to observe

any change in instrument throughput (Bhartia et al. 2021). This spectrum also includes the 252.93 nm laser emission line, which can be used for the analysis of laser health (Uckert et al. 2021) along with an internal photodiode. These reflectance and emission lines are used to check for changes in laser energy and spectrometer wavelength calibration by monitoring significant deviations in the reported peak wavenumber of either band over time.

The SCT is expected to be measured approximately every 180 sols, or as needed, after potential sample analysis anomalies. Measurements of the SCT targets are obtained using a standard calibration sequence with occasional modifications due to rover resources such as power, data availability, and time of day. They typically consist of a 10×10-point spectral map with 780 μm spacing between points and 10 pulses per point. An ACI image is acquired before and after each raster to evaluate any RA drift. The maze and meteorite targets are measured using a 36×36-point map (200 μm spacing) to characterize laser position accuracy.

Over the course of the mission, dust from airfall, dust storms, and dust devil events will be deposited on or removed from rover hardware (Cousin et al. 2015; Berger et al. 2016; Schmidt et al. 2015; Yingst et al. 2020), including the SCT. Images of the SCT taken by WATSON already show that dust has accumulated on the protective umbrella, the aluminum faceplate, as well as on the surface of and in the well edges of the calibration targets (Figs. 5, 6). As the mission progresses, we will continue to monitor dust accumulation during instrument calibration, including investigations of how measured spectral intensities are modified by attenuation of the SHERLOC laser through the dust coating different targets. Differences in the mineralogical composition may be attenuated and could be harder to detect, particularly if there is significant UV absorption due to the iron-rich nature of the dust (Carrier et al. 2019).

3 Instrument Calibration Operations

3.1 Calibration Data Collected Prior to Flight

Pre-flight calibration of the SHERLOC FM is described elsewhere (Bhartia et al. 2021). In brief, these tests were performed within an environment chamber at JPL with the FM attached to the flight RA. Tests and calibrations included defining arm placement, obtaining imaging mosaics, internal calibration of the AlGaN target on the dust cover, spectrometer/ACI axial alignment and spectral peak positions of various targets including all the targets on the SCT. All aspects of the instrument worked at or exceeded scientific requirements.

Prior to launch, the SCT targets were spectrally characterized using MOBIUS (Mineral and Organic Based Investigation with Ultraviolet Spectroscopy), a custom DUV Raman/fluorescence spectrometer at JPL. MOBIUS differs from SHERLOC in terms of spectral resolution, sensitivity, and laser spot size (Razzell Hollis et al. 2021b), but spectra are similar enough to allow direct comparison between pre- and post-landing to validate and refine the SHERLOC calibration.

3.2 Calibration Data Collected on Mars

The SCT palette was first examined on Mars using WATSON on Sol 26 (Figs. 5, 7) and by the spectrometer and ACI on Sol 27 as part of the rover's Surface Operations Transition (SOX) checkout. Subsequent analyses during the rover's first 200 sols on Mars were performed on Sol 59 (ACI), 62 (WATSON), and 181 (ACI). The Sol 181 observations were acquired at night; the other observing sessions were performed during daylight conditions.

Fig. 5 WATSON image mosaics of the SCT acquired on Sol 26 (top) and 62 (bottom). The Sol 26 mosaic was illuminated by the sun from the top right; the Sol 62 mosaic was acquired with the SCT in full shadow. Both are mosaics of 3 WATSON images acquired from about 12 cm distance (about 51.0 ± 2.5 μm/pixel)

The Sol 26 WATSON images showed the SCT to have accumulated, as expected based on MSL's MAHLI calibration target experience (Edgett et al. 2015; Yingst et al. 2020), a thin coating of dust that was emplaced during the rover's terminal descent on Sol 0 (Fig. 6). These initial ACI images and spectra of the SCT were taken on Sol 27 and indicated nominal instrument performance, in agreement with pre-launch measurements. However, ACI autofocus, for each target, was accidentally commanded in a manner that resulting images and spectrometer laser were not in focus, thus the ACI and spectrometer measurements had to be redone.

The initial calibration sequence was re-commanded successfully on Sol 59 and is described here. Figure 7 shows a mosaic of three WATSON images of the SCT acquired with the camera front lens element about 12 cm from the target (spatial scale of 50.7 ± 2.5 μm/pixel). The grayscale images overlaid on the WATSON image in Fig. 7 are the 10.1 μm/pixel ACI images obtained on Sol 59.
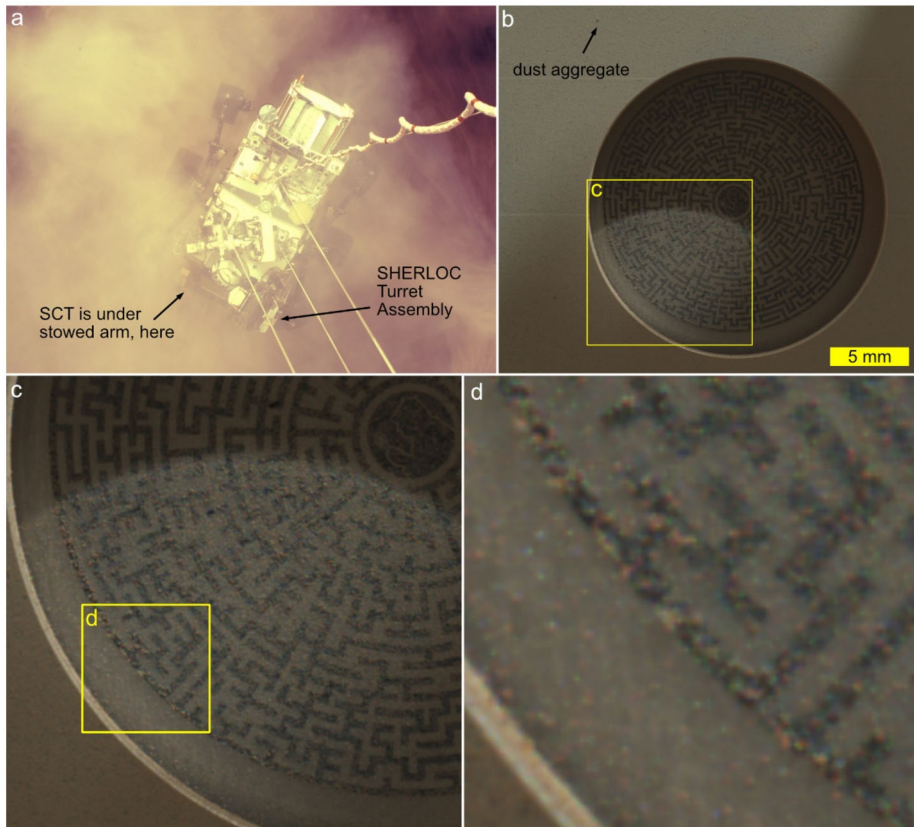
Fig. 6 The SCT was coated with a thin film of dust and dust aggregates during the rover's terminal descent to the Martian surface on Sol 0. (**a**) Descent Stage Downlook Camera (Maki et al. 2020) view of dust raised by terminal descent engines during landing in February 2021. (**b**) SCT intensity maze target as viewed by WATSON on Sol 26; note example (arrow) sand-sized dust aggregate. (**c**) Closer view of the intensity maze target viewed by WATSON on Sol 26. (**d**) expanded view showing dust aggregates on the intensity maze; spacing between black chrome maze features is 200 μm

A standard measurement protocol was applied for all SCT target measurements. At each target, the ACI is first focused by acquiring an ACI autofocus sub-frame, 256 × 256 pixels at the center of the field of view. Autofocus establishes a stepper motor count position that is then used to obtain a full-size ACI image (1648 by 1200 pixels) to document the scene. The ACI images of the SCT are acquired with both groups of white light LEDs illuminated. There is a slight offset between optimum focus of the ACI and that of the spectrometer, so the best focus position of the laser requires the motor count position determined by best focus. The focus position determined by ACI autofocusing has to be adjusted by 150 motor steps in order to focus the laser.

Then, a 7 × 7 mm spectral map is collected, with a 10 pulses per point scan applied to most targets, and a higher resolution 36 × 36-point scan employed for the maze and meteorite targets. Measurements of the maze target are used to validate the laser position at the surface, and the meteorite target contains small-scale features that may be missed with a coarsely-spaced laser spot pattern, necessitating more detailed spectral maps in both cases. Each spectrometer raster scan is followed by an additional ACI autofocus subframe
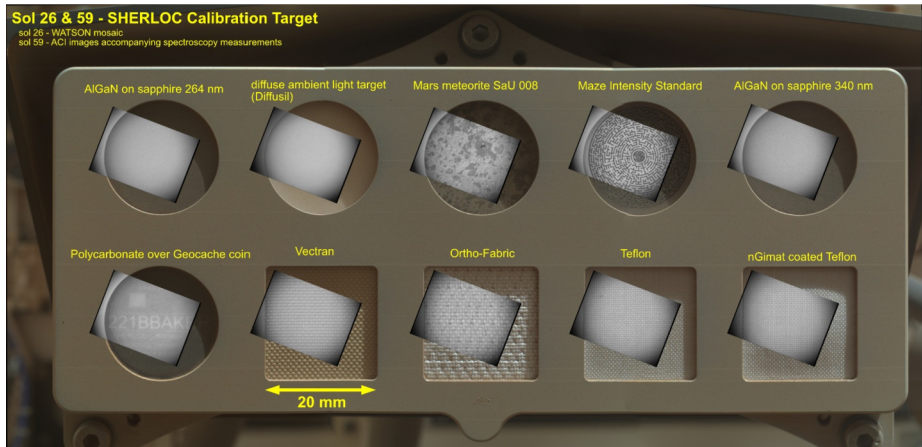
Fig. 7 WATSON image mosaic of the SCT obtained on Sol 26 overlain with ACI full-frame (1648 by 1200 pixels) camera images obtained on Sol 59. The WATSON mosaic was obtained at a standoff distance of 12 cm with a resolution of 51 micron/pixel while the ACI was obtained through a commanded standard standoff of 48 mm with 10.1 micron/pixel resolution. These images show the condition of SCT targets shortly after landing. Yellow annotations were added to the figure to identify individual targets
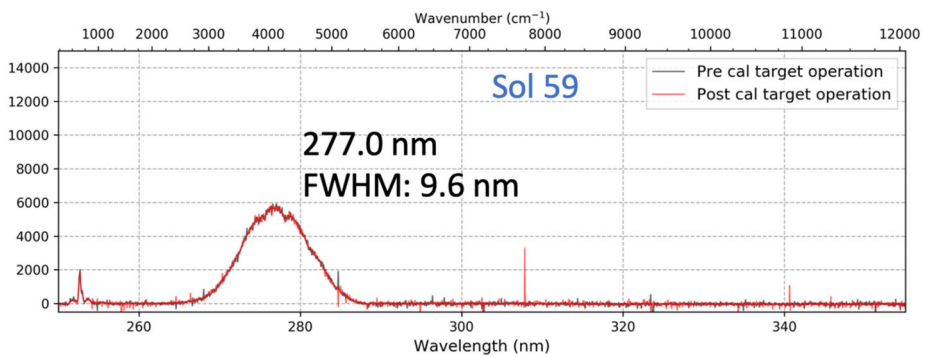

Fig. 8 Spectra of the SHERLOC internal AlGaN calibration target on Sol 59 before (black trace) and after (red trace) the external calibration measurement, showing consistent spectral alignment and negligible laser power drop after the calibration suite measurements

(centered, 256 by 256 pixels) and a full-frame ACI (1648 by 1200 pixels) view to document any RA drift (in three dimensions) that might have occurred during the spectrometer measurements.

A downlink assessment of each measurement is conducted as data arrive on Earth; for the spectrometer, this includes cosmic ray removal, laser normalization, registration of laser shots on images, peak fitting, spectral intensity map generation, and instrument state-of-health assessment. A summary of the results from each of the calibration target measurements is provided in the subsections that follow.

Internal AlGaN (277 nm) We acquire a spectrum of the internal AlGaN target before every SHERLOC observation in order to monitor laser health (Fig. 8). This is done with the cover closed at a manual stepper motor focus position of 4500. At this focus position, the spectra
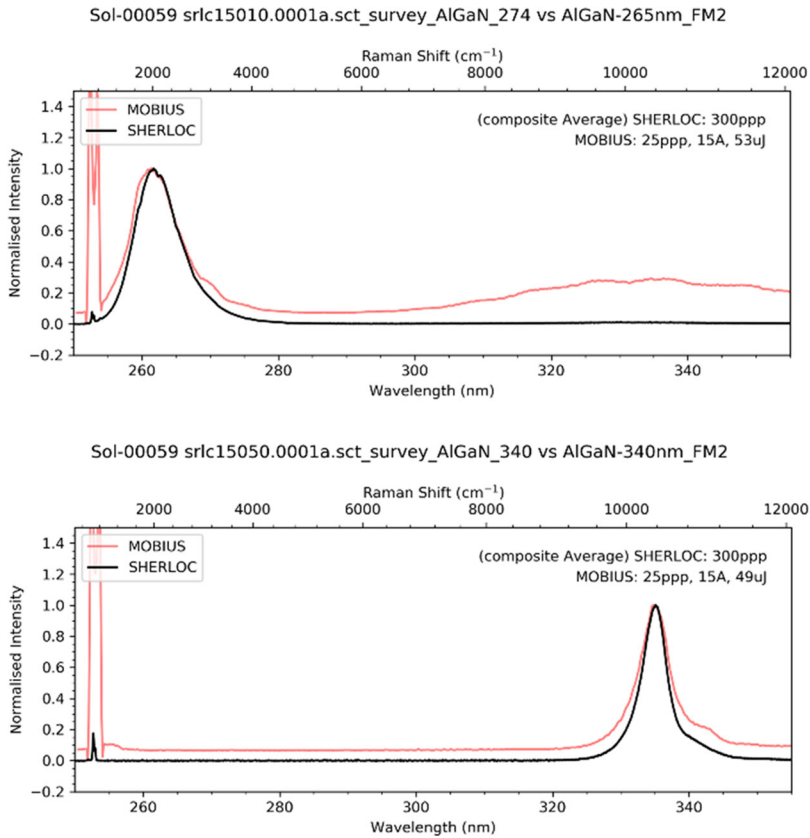
Sol-00059 srlc15010.0001a.sct_survey_AlGaN_274 vs AlGaN-265nm_FM2

Sol-00059 srlc15050.0001a.sct_survey_AlGaN_340 vs AlGaN-340nm_FM2

Fig. 9 Normalized spectra for the two AlGaN targets taken with SHERLOC on Sol 59 in black, with pre-launch values taken on MOBIUS in red

are out of optimum focus, but the data obtained are sufficient to compare laser power over multiple deployments. Figure 8 shows a spectrum of the internal calibration target, showing the AlGaN Raman signature at 277 nm. This spectrum was collected using 300 laser shots in a single position, showing consistent alignment and signal throughput before and after the calibration activities, also consistent with pre-launch spectra.

AlGaN for Raman (264 nm) and Fluorescence (340 nm) Measurements of the external AlGaN calibration targets with high responses in the Raman (264 nm) and fluorescence (340 nm) ranges were consistent with pre-launch measurements (Fig. 9). The 7×7 mm spectral maps show some signal attenuation in a ~ 1 mm^2 patch in both targets, likely due to a higher accumulation of dust in these areas.

Diffuse Transmission Target The DT target was measured using a 10 mm $\times$ 10 mm map, and the resulting spectra are consistent with pre-launch measurements; several peaks in the Raman region and a broad fluorescence background are observed. Figure 10 shows the spectra of the DT before and after landing. The DT target exhibits a broad, relatively weak fluorescence feature centered at 275 nm, which was apparent in pre-launch measurements. In the Raman region, there are four major peaks at 503, 800, 1069 and 1190 cm^{-1} that are variously assigned to bending and stretching modes of fused silica.
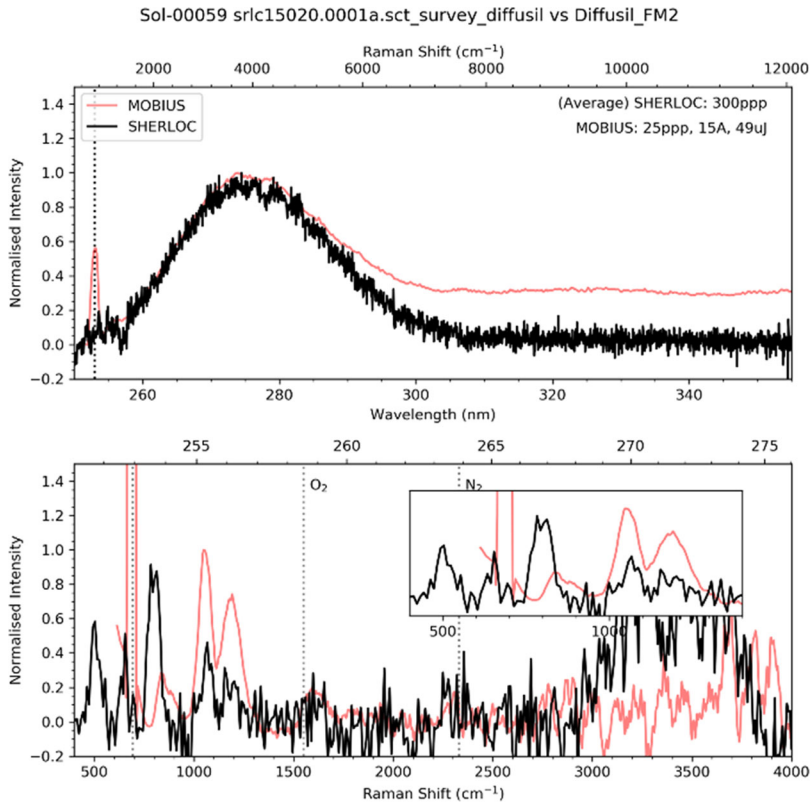
Fig. 10 Spectra of the DT target, with red lines indicating pre-launch measurements using MOBIUS, while black lines are the spectra taken by SHERLOC on Sol 59. Top spectrum is the fluorescence region, and bottom is the Raman region. The peak at 252.9 nm is the secondary laser line

The 450 and 800 cm^{-1} peaks could not be resolved in the pre-launch spectrum as they are cut off by the MOBIUS instrument's edge filter, which significantly attenuates the observed signal below 800 cm^{-1} ($\sim$253.6 nm). The positions of the 1069 and 1190 cm^{-1} peaks were difficult to estimate due to relatively low signal in the SHERLOC spectrum, which may account for deviation from their corresponding positions (1055 and 1188 cm^{-1}) in the higher signal, pre-measurement spectrum.]

Geocache Coin Target Spectra of the geocache target were weaker than measurements from pre-launch, but still contain the characteristic polycarbonate Raman peak and broad fluorescence background expected. The ACI autofocused on the dust-coated polycarbonate surface, rather than the underlying opal geocache coin, resulting in spectral measurements of the polycarbonate attenuated by dust. The dust had largely been emplaced from fines entrained by the rover's descent engines during landing (Fig. 6). The ACI images collected before and after the spectroscopy measurements were differenced (Fig. 11), revealing dust movement induced by the SHERLOC laser. The most likely reason for this dust movement is the laser changing the electrostatic charge of the dust particles adhering on the target. Electrostatic effects have been shown to occur with any movement of dust on the martian surface (Anderson et al. 2009; Beegle et al. 2009). The annulus-shaped absence of dust in the ACI image

Fig. 11 Sol 59 ACI image of martian dust-coated polycarbonate spacesuit visor sample over geocache coin (left). Scale Reference: total target diameter is 25 mm; ACI images are full-frame images (1648 by 1200 pixels) acquired before and after the laser is fired, aligned, and subtracted. Bright spots in the right image represent differences in the target after the laser was fired, revealing dust mobilization

acquired after the spectroscopy measurements was used to validate knowledge of laser position relative to the ACI field of view, the laser spot size and shape, and provides a means to evaluate the robotic arm drift throughout the measurement, which proved to be negligible over this time period.

The geocache/polycarbonate target exhibits a broad fluorescence spectrum that is roughly similar in shape to pre-launch measurements (Fig. 12). The Raman region shows the characteristic polycarbonate peak at 1602 cm^{-1}, compared to 1598 cm^{-1} in the pre-launch measurement. The position discrepancy of -2.3 cm^{-1} is well within the expected combined uncertainty of the SHERLOC calibration and peak fitting.

Martian Meteorite Two maps were collected on the SaU 008 martian meteorite target, a 1296 point survey and a 100 point high dynamic range (HDR) scan, with different laser exposures (15 and 300 pulses per point, respectively) and spatial resolutions (140 and 780 μm, respectively) to assess SHERLOC's ability to detect spectral features and resolve spatial distributions associated with chemical composition under typical operating conditions. Pre-launch and post-landing measurements of the meteorite are shown in Fig. 13. Pre-launch measurements included a coarse (500 μm spacing) fluorescence map covering the entire target, and high resolution (100 μm) Raman and fluorescence maps of the target center, all of which overlap with the area scanned by SHERLOC, as illustrated in Fig. 13c.

Pre-launch intensity maps show that the meteorite surface has a single, dominant fluorescence signature, with a maximum around 340 nm (appearing red in the Fig. 13 maps), which is generally stronger in lighter toned regions and weaker in darker toned regions. A small natural void (vug) is visible in the meteorite (Figs. 3c and 13) with dimensions of ∼1-2 mm^2 in area and 1 mm depth. It has a particularly strong, broad fluorescence signature (appearing bright yellow in the spectral maps). This feature is an excellent landmark, appearing near the center of the target and having an extremely strong, distinctive fluorescence spectrum that is visible in both pre-launch and post-landing measurements. The survey scan from Sol 181 (Fig. 13e) shows that SHERLOC is not just capable of detecting the distinctive signature of the vug, but also the strong ∼340 nm fluorescence from a network of pale, narrow lines in the surrounding material. These lines appear to be about 20–30 μm thick, based on ACI imagery, but are still well resolved in the survey scan, as the diameter of the SHERLOC laser spot (∼100 μm) is comparable to the spacing between points in the map (140 μm), ensuring good coverage of the scanned area.
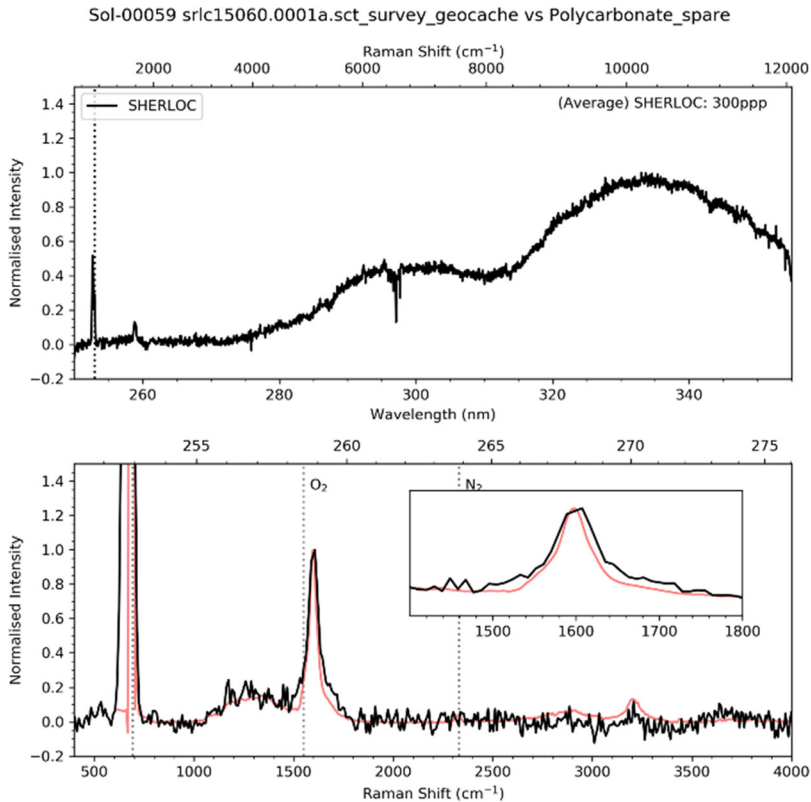
Fig. 12 Raman spectra gathered on Sol 59 of the geocache/polycarbonate targets (in black), compared to spectra taken prior to launch in red and of spare material (Brassboard). Raman regions are shown after polynomial baseline subtraction

In terms of Raman scattering, the meteorite exhibits multiple detectable Raman bands associated with either mineralogy or organic material (Fig. 13g). Organic material is apparent by a broad D band at ∼1370 and a strong G band at ∼1600 cm^{-1}, typical of macromolecular carbon. Multiple mineral phases can be identified by narrowing, overlapping peaks between 900 and 1100 cm^{-1}, including phosphate (∼960 cm^{-1}), pyroxene (∼1010 cm^{-1}), and calcium carbonate (∼1080 cm^{-1}). The carbonate could have formed during terrestrial alteration in the Omani desert. Based on pre-launch measurements, the light-toned regions of the meteorite are pyroxene-rich and provide the strongest signal at 1010 cm^{-1}, while the vug is associated with the strongest carbonate and organic signatures, consistent with its fluorescence. The overall signal intensity was lower than pre-launch measurements due to differences in the number of laser pulses used, instrument throughput, and dark noise, and signal attenuation by martian dust that has accumulated on the target since landing. Assessing the spatial distribution of Raman peak intensities across the survey scan area is difficult due to weak signal resulting from the low number of laser pulses used at each location (15 pulses per point). Using more pulses, such as in the HDR scan (300 pulses per point) enables detection of Raman peaks from individual spectra, but at lower spatial resolution, while the mean spectrum for the entire scan provides the best possible signal-to-noise-noise ratio. In the mean spectrum, the relative intensity of the pyroxene peak versus the organic G band
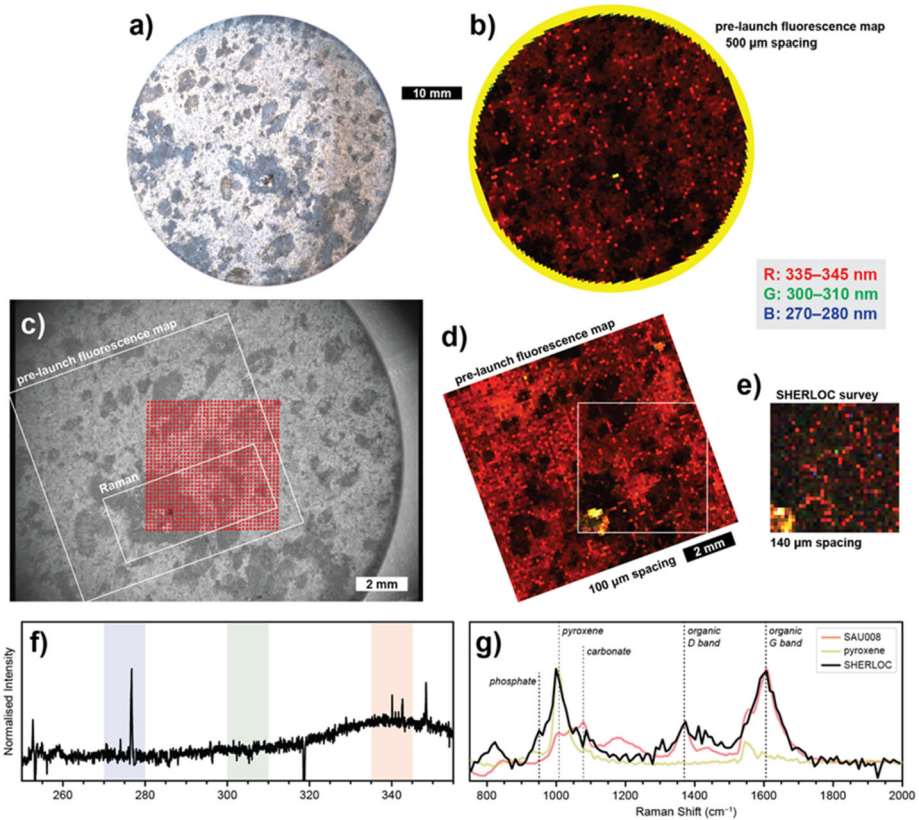
Fig. 13 **a**) Color photograph of SaU 008 meteorite taken before launch, **b**) coarse DUV fluorescence map taken prior to launch using the MOBIUS instrument, at 50 laser pulses per point and 500 μm spacing between points. **c**) Sol 181 ACI image of the meteorite, annotated to indicate areas scanned before launch (white rectangles) and the individual points scanned by the SHERLOC survey activity (red dots). **d**) A fluorescence map taken before launch at higher resolution (100 μm). **e**) A fluorescence map for the SHERLOC survey on Sol 181 (1296 points, 15 pulses per point, 140 μm spacing). **f**) The mean fluorescence spectrum of the survey map, with red, green, and blue wavelength channels highlighted. **g**) The mean Raman spectrum of the SHERLOC HDR map (100 points, 300 pulses per point, 780 μm spacing) after polynomial baseline subtraction, compared to the mean spectrum taken prior to launch and a pyroxene standard (enstatite) measured on MOBIUS. Fluorescence intensity maps are normalized to the 2nd and 98th percentile values

is significantly higher than in pre-launch measurements, likely the result of the SHERLOC scan covering a different area with a greater proportion of light-toned, pyroxene-rich material.

As the mission progresses, measurements of the martian meteorite can be used to routinely assess SHERLOC's scientific functionality using a realistic, Mars-relevant sample that contains a known spatial distribution of mineral phases and abiotic organic material. Should the capability of SHERLOC to detect one or more of these components decrease during the mission, the meteorite may be used to re-optimize measurement parameters to ensure the best practical scientific return under surface operation conditions.

Intensity Maze A 1296-point spectral map was collected on the fused silica glass maze target to validate the laser position accuracy relative to the ACI context images. This also
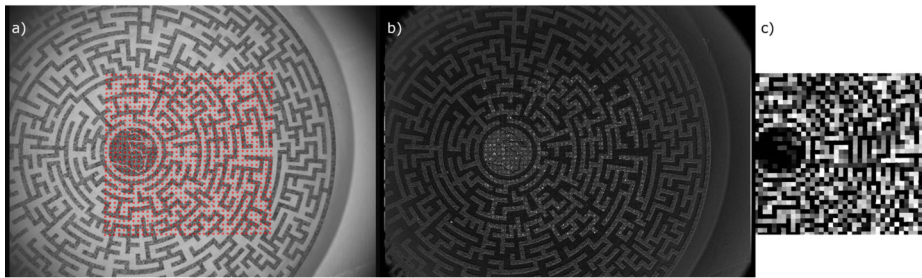
Fig. 14 **a**) An ACI image of the SHERLOC maze target acquired on Sol 59, with red annotations indicating the calculated laser shot positions. **b**) A differenced image of the maze target, with bright spots indicating the laser shots, evidencing dust removal from the surface by the laser. **c**) A fluorescence intensity map of the SHERLOC maze target

enabled assessment of RA drift during the measurement. Similar to the dust removal effect described with the geocache coin, a differenced image of the pre- and post-spectroscopy ACI images shown in Fig. 14 indicates the position and shape of the laser spots in the ACI image and is used to verify laser positioning. The pre- and post-ACI images were used to show minimal RA drift during the ∼20-minute observation. The spectral intensity map shown in Fig. 14 shows the high fluorescence (white) and low fluorescence (black) regions of the spectral map, closely matching the expected laser shot positions. The fused silica glass fluoresces more than the chrome coating, resulting in a lower resolution UV fluorescence image of the target that can then can be aligned to the ACI image to verify the spectrometer to laser mapping to ACI boresight.

As shown in Fig. 15, an additional analysis enabled by the maze target is an intensity assessment to confirm beam size and instrument performance. Given the difference images of a dust-coated SCT target, the beam size evaluation is no longer relevant, but may become so in future observations if dust has been removed from the SCT. However, for instrument performance, a high-resolution line scan (∼25 μm spacing) across a few of the chrome lines provides a sinusoidal pattern of reflected laser light. As the ∼110 μm diameter laser beam crosses from the glass to the chrome, the intensity of the fluorescence and/or Raman will be proportional to the fraction of the beam on the glass. If the laser beam and the spectrometer slit are misaligned, the proportionality will change. These data can be used to tailor the spectroscopy operations parameters to mitigate small misalignments that may occur over the course of the mission.

Spacesuit Materials Each of the four spacesuit materials were analyzed by SHERLOC, with autofocus subframe ACI images shown in Fig. 4, and described in detail below.

Teflon-Based Materials The three Teflon-based spacesuit materials (Teflon, nGimat-coated Teflon, and Ortho-Fabric) exhibit similarly broad fluorescence, with maxima around 332 nm (Fig. 16). In the Raman region, all three materials exhibit similar spectra, with a single peak around 730 cm^{-1} and a set of three Raman peaks around 1210, 1298, and 1380 cm^{-1}, all of which are characteristic of Teflon. For pure Teflon, the peaks were at 731, 1210, 1298, and 1374 cm^{-1}; for nGimat-coated Teflon, the peaks were at 731, 1210, 1298, and 1374 cm^{-1}; and for Ortho-Fabric the peaks were at 731, 1211, 1299, and 1376 cm^{-1}.

The spectra appear almost identical to pre-launch measurements, relative intensities of the different peaks are the same, although the peaks are broader due to the lower spectral resolution of SHERLOC compared to the MOBIUS instrument (Razzell Hollis et al.
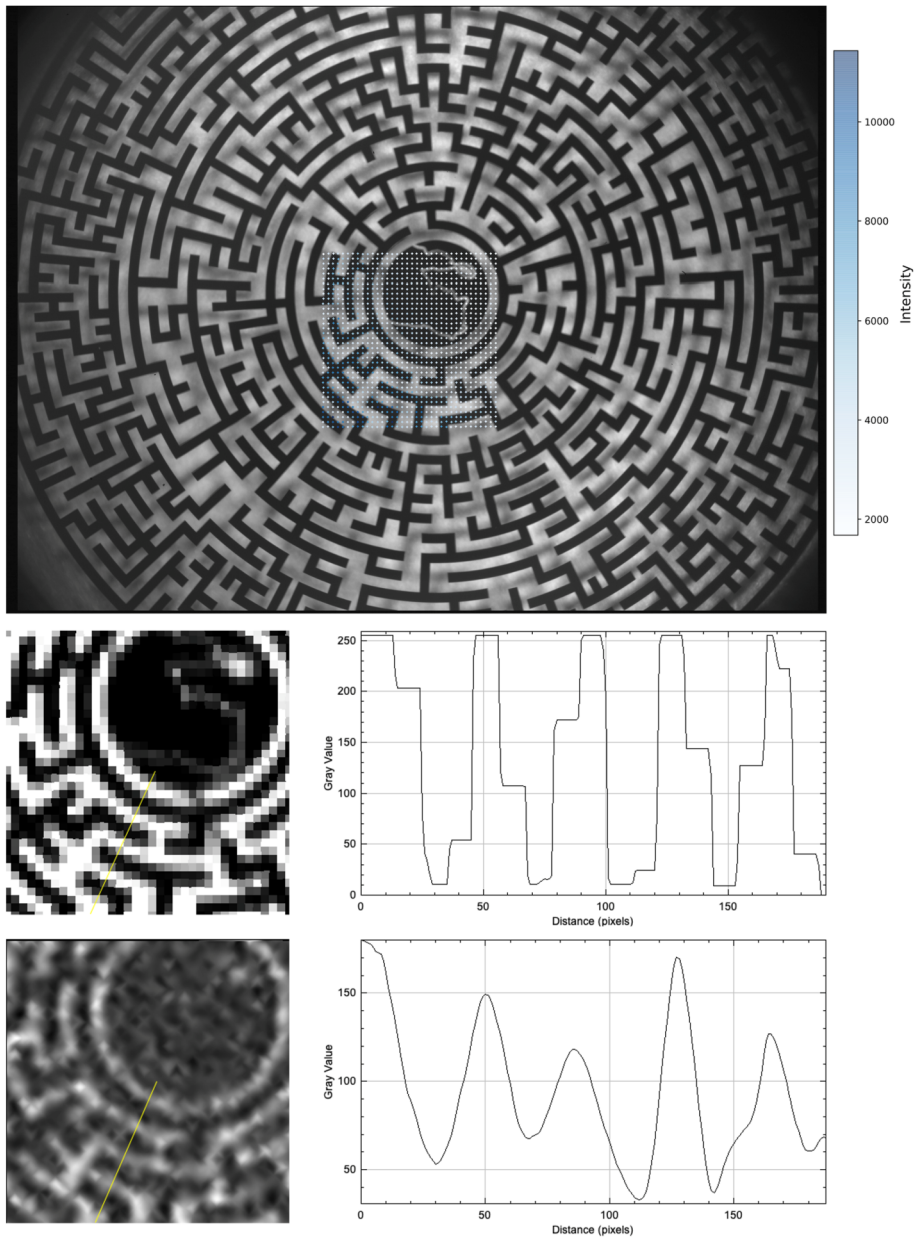
Fig. 15 Image of the Maze target simulating how a scan across the maze target would appear. As the laser beam crosses from the glass to the chrome, the intensity of the fluorescence and/or Raman will be proportional to the fraction of the beam on the glass and approximate a sinusoidal pattern

2021b). We were unable to resolve the ~730 cm^{-1} peak in pre-launch measurements, but fitted peak positions for the Teflon triplet were shifted between -2 and $+5$ cm^{-1} compared to pre-launch values for the same targets, which is within the expected uncertainty of the
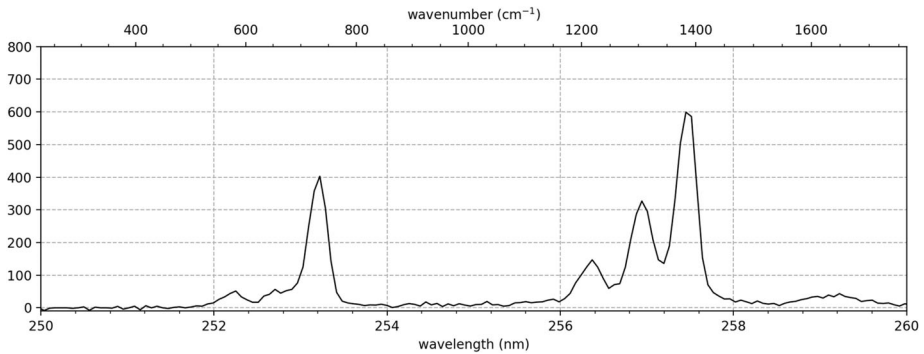
Fig. 16 Raman spectrum of the Teflon target taken on Sol 59 on Mars

SHERLOC calibration and peak fitting. Some of this variation is due to the difference in sample temperature between the pre-launch measurements (done under room temperature) and surface measurements (done under local martian conditions), as sample temperature can alter the observed frequency for a given vibrational mode.

Vectran Material The Vectran target (Fig. 17d) exhibits little fluorescence and a relatively weak Raman spectrum with several overlapping peaks between 1000 and 1800 cm^{-1}, with the most distinctive peaks occurring at 1150, 1375, and 1594 cm^{-1}. The spectrum appeared identical to pre-launch measurement, albeit with a lower signal-to-noise ratio. Fitted peak positions were within 7 cm^{-1} of pre-launch values, within expected uncertainty of calibration and peak fitting.

3.3 Aeolian Dust on the SCT

Although aeolian dust has accumulated on all parts of the SCT (e.g., Fig. 6), we have observed that the dust is visually and spectrally more pronounced on certain targets (polycarbonate) over others. At present, we can only provide a first-order qualitative assessment of the dust accumulation on each of the calibration targets due to several unknown factors, such as lighting and distance from the target. These initial observations have important considerations for spacesuit material selection in future human exploration activities on the martian surface. In particular, if the polycarbonate material, which is the material selected for astronaut helmet visors, suffers from increased dust accumulation this could impact visibility.

3.4 Recalibration

One of the purposes of the SCT is to monitor the spectral calibration of the SHERLOC instrument and to ensure that we can confidently report Raman and fluorescence peak positions to an accuracy needed for mineralogical and organic compound identification. The original spectral calibration described in Uckert et al. 2021 was determined prior to integration of SHERLOC onto the rover, and uses two quadratic functions, one for the Raman region (pixels 0–499) and one for the fluorescence region (pixels 500–2147). The initial results from the SCT revealed a slight change in calibration for the Raman region, which was calculated from the available SCT data and used to correct all of the Raman spectra shown in this article.
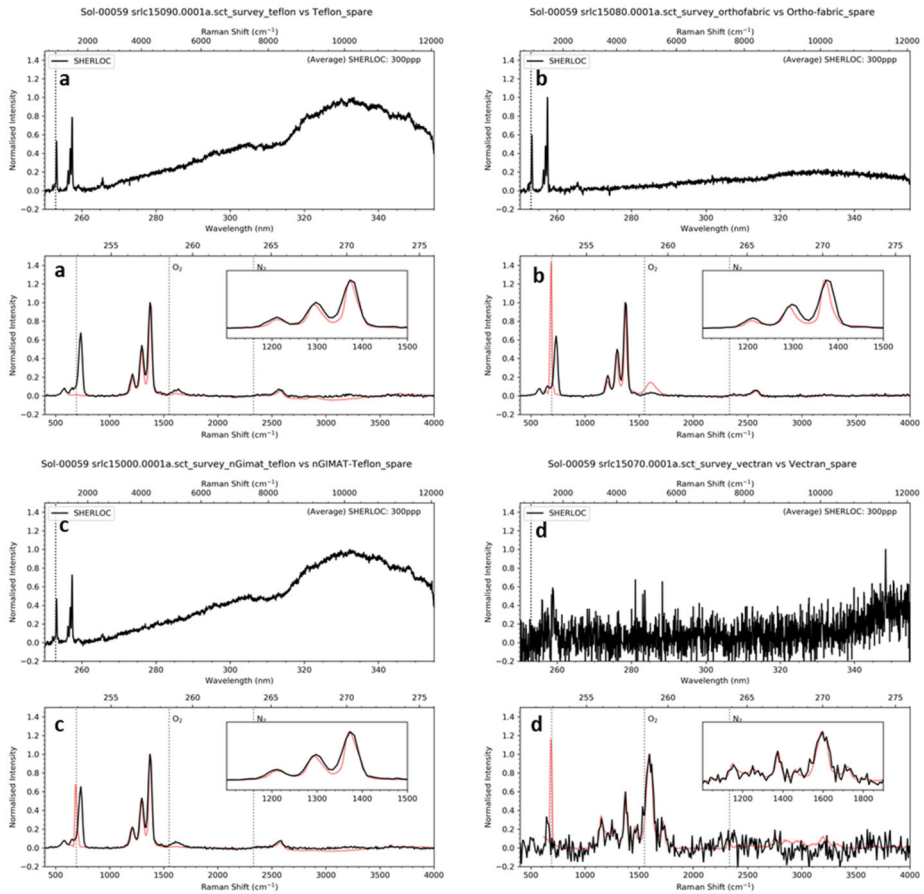
Fig. 17 The normalized mean spectra for Teflon (**a**), Ortho-Fabric (**b**), nGimat-coated Teflon (**c**), and Vectran (**d**) targets taken by SHERLOC on Sol 59 (black lines), compared to spectra taken prior to launch using MOBIUS (red lines). Raman regions are shown after polynomial baseline subtraction

The change in calibration was first observed on Sol 59 as a discrepancy in Raman peak positions for the material targets versus pre-launch measurements taken on MOBIUS (see Fig. 18). The average discrepancy was $\sim$10 cm^{-1}, equivalent to $\sim$0.08 nm, or approximately 1 pixel on the SHERLOC SCCD, but varied across the accessible spectral range between 650 and $\sim$1600 cm^{-1} (92.3 to 190.4 pixels). The magnitude of the discrepancy appeared to vary significantly between individual peaks, even in the same sample, with the Teflon triplet moving by $+3.3$, $+11.1$, and $+9.5$ cm^{-1}. Some of the discrepancy is due to the calibration targets being at a lower temperature on Mars, as pre-launch System Thermal Testing (STT) of SHERLOC showed the Teflon triplet moved by -1.3, $+7.7$, and $+5.1$ cm^{-1} under diurnal temperature ranges expected of the target on Mars. We accounted for temperature by experimentally measuring the change in Raman peak positions for each material between $+20\,°C$ and $-100\,°C$. Assuming an average SCT temperature of $-50\,°C$, the triplet of Teflon-based materials will move by -2.7, $+4.2$, and $+1.1$ cm^{-1}, the three major peaks of Vectran move by -5.0, $+0.5$, and $+0.0$ cm^{-1}, and the single peak of polycarbonate moves by $+2.4$ cm^{-1}.
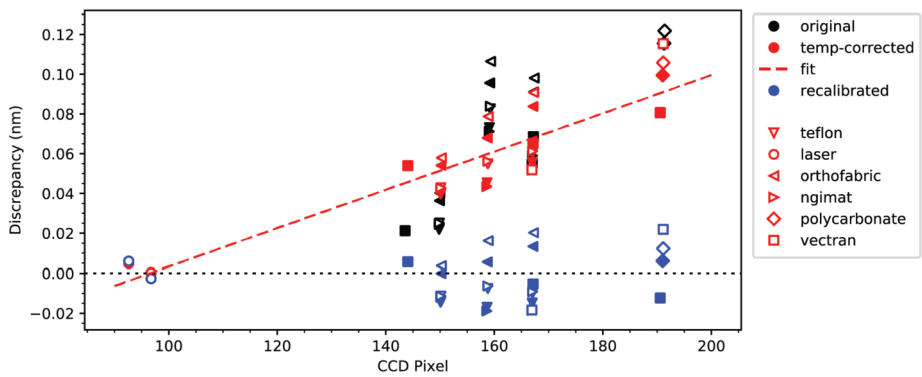
Fig. 18 Raman peak position discrepancies for the Teflon target from Sol 59 using the original calibration (black points), before and after temperature correction. Position discrepancies for Teflon (inverted triangles) from pre-launch System Thermal Testing (STT) using the original calibration (black points), before and after temperature correction (red points). Position discrepancies for all calibration targets on Sols 59 and 181, comparing the old calibration and the new calibration (after temperature correction; blue points). All discrepancies are versus pre-launch values acquired on MOBIUS

However, when peak positions are corrected to account for temperature, we still observe a discrepancy between surface and pre-launch values.

In order to confirm the change in calibration, we assessed the Raman peak positions of the following targets: Teflon, nGimat-coated Teflon, Ortho-Fabric, Vectran, and polycarbonate, measured on Sols 59 and 181. We also included two known laser emission lines that were visible in most spectra: a plasma line at 252.6592 nm (649.2 cm^{-1}), and a lasing line at 252.93048 nm (692.0 cm^{-1}), the positions of which should also reflect any change in calibration. Figure 18 shows the observed discrepancy in peak positions (expressed as wavelengths, in nm) after correcting for temperature, demonstrating that discrepancy increases monotonically and in a roughly linear fashion between ∼650 and ∼1600 cm^{-1} (92.3 to 190.4 pixels), with the line of best fit represented by the dashed red line in Fig. 18. Given the quadratic nature of the SHERLOC calibration, it is likely that the discrepancy follows a quadratic curve as well, but we could not reliably infer any non-linearity from the relatively narrow range of positions we could assess. By subtracting the linear fit from the original calibration reported by Uckert et al. 2021, we were able to derive a new calibration for converting pixel numbers to wavelength (equation (1)). This applies specifically to the Raman region of the detector (where pixel number $x < 500$), the calibration of the fluorescence region ($x \geq 500$) remains unchanged.

$$\left(-7.85 \times 10^{-6}\right) x^2 + \left(6.524 \times 10^{-2}\right) x + 246.69, \quad x < 500 \tag{1}$$

When the new calibration is applied, the overall discrepancy in Raman peak positions is reduced, from an average of +9.6 ± 6.6 cm^{-1} to 0.0 ± 1.8 cm^{-1}, and no longer varies monotonically across the spectrum. There was little difference between Sols 59 and 181, indicating that the system is stable over long periods of time and is not significantly affected by vibrations from use of the percussive drill. Future calibration target measurements will assess this stability over time. Even if temperature is not accounted for, recalibrated peak positions are on average +0.7 ± 3.1 cm^{-1} from their pre-launch positions. This represents an improvement in calibration and should increase the scientific return from SHERLOC observations, as the ability to measure peak positions with greater accuracy will enable

more reliable and precise identification of minerals and organic compounds from observed spectra (Razzell Hollis et al. 2021b).

4 Summary

The SHERLOC Calibration Target (SCT) is a sophisticated, compact, and science-rich device that meets all SHERLOC science, contamination control, and engineering requirements imposed by the Mars 2020 mission. It also enables science investigations that address the nature and behavior of carbon and organic compounds in the martian surface environment, future engineering challenges pertaining to the expected service lifetimes of spacesuit materials, and it provides a rich suite of education and public outreach (EPO) tools that include the first geocache deployed on another planet.

The SCT was fully characterized by a SHERLOC analog instrument in the laboratory and in the testbed prior to launch. These spectra have been compared to those obtained during the analysis of the SCT on Sols 27, 59 and 181. This comparison shows very little change in peak position and intensity for key calibration targets including the AlGaN target positioned on the interior of the dust cover. Through these detailed analyses and comparisons, we were able to better refine the initial SHERLOC calibration to take advantage of the stability of the features in each of these targets.

References

J.H. Allton, J.D. Hittle, E.T. Mickelson, E.K. Stansbery, *Cleaning Genesis Sample Return Canister for Flight: Lessons for Planetary Sample Return*. Astromaterials Research & Exploration Science (2002). https://ntrs.nasa.gov/api/citations/20160002409/downloads/20160002409.pdf?attachment=true

R.C. Anderson, L.W. Beegle, G.H. Peters, G.M. Flemming II., L. Jandura, K. Kreichbaum, K. Manatt, A. Okon, E. Pounders, L. Sollitt, D. Sunshine, Particle transport and distribution on the Mars Science Laboratory mission: effects of triboelectric charging. Icarus **204**(2), 545–557 (2009). https://doi.org/10.1016/j.icarus.2009.07.006

D. Barnes, M. Wilding, M. Gunn, L. Tyler, S. Pugh, A. Coates, A. Griffiths, A. Cousins, N. Schmitz, G. Paar, The PanCam Calibration Target (PCT) and multispectral image processing for the ExoMars 2018 mission, in *EPSC-DPS Joint Meeting*, vol. 289 (2011), p. 2011

L.W. Beegle, G.H. Peters, R.C. Anderson, R. Bhartia, A.G. Ball, L. Sollitt, Particle sieving and sorting under simulated Martian conditions. Icarus **204**(2), 687–696 (2009). https://doi.org/10.1016/j.icarus.2009.07.008

L.W. Beegle, R. Bhartia, M. White, L. DeFlores, W. Abbey, Y.-H. Wu, B. Cameron, J. Moore, M. Fries, A. Burton, K.S. Edgett, M.A. Ravine, W. Hug, R. Reid, T. Nelson, S. Clegg, R. Wiens, S. Asher, P. Sobron, SHERLOC: scanning habitable environments with Raman & Luminescence for organics & chemicals, in *2015 IEEE Aerospace Conference* (IEEE, Big Sky, 2015). https://doi.org/10.1109/AERO.2015.7119105

J.A. Berger, M.E. Schmidt, R. Gellert, J.L. Campbell, P.L. King, R.L. Flemming, D.W. Ming, B.C. Clark, I. Pradler, S.J.V. VanBommel, M.E. Minitti, A.G. Fairén, N.I. Boyd, L.M. Thompson, G.M. Perrett, B.E. Elliott, E. Desouza, A global Mars dust composition refined by the Alpha Particle X-ray Spectrometer in Gale crater. Geophys. Res. Lett. **43**, 67–75 (2016). https://doi.org/10.1002/2015GL066675

R. Bhartia, L.W. Beegle, L. DeFlores, W. Abbey, J. Razzell Hollis, K. Uckert, B. Monacelli, K.S. Edgett, M.R. Kennedy, M. Sylvia, D. Aldrich, M. Anderson, S.A. Asher, Z. Bailey, K. Boyd, A.S. Burton, M. Caffrey, M.J. Calaway, R. Calvert, B. Cameron, M.A. Caplinger, B.L. Carrier, N. Chen, A. Chen, M.J. Clark, S. Clegg, P.G. Conrad, M. Cooper, K.N. Davis, B. Ehlmann, L. Facto, M.D. Fries, D.H. Garrison, D. Gasway, F.T. Ghaemi, T.G. Graff, K.P. Hand, C. Harris, J.D. Hein, N. Heinz, H. Herzog, E. Hochberg, A. Houck, W.F. Hug, E.H. Jensen, L.C. Kah, J. Kennedy, R. Krylo, J. Lam, M. Lindeman, J. McGlown, J. Michel, E. Miller, Z. Mills, M.E. Minitti, F. Mok, J. Moore, K.H. Nealson, A. Nelson, R. Newell, B.E. Nixon, D.A. Nordman, D. Nuding, S. Orellana, M. Pauken, G. Peterson, R. Pollock, H. Quinn, C. Quinto, M.A. Ravine, R.D. Reid, J. Riendeau, A.J. Ross, J. Sackos, J.A. Schnaffer, M. Schwochert, M.O. Shelton, R. Simon, C.L. Smith, P. Sobron, K. Steadman, A. Steele, D. Thiessen, V.D. Tran, T. Tsai, M. Tuite, E. Tung, R. Wehbe, R. Weinberg, R.H. Wiener, R.C. Wiens, K. Williford, C. Wollonciej, Y.-H. Wu, R.A. Yingst, J. Zan, Perseverance's Scanning Habitable Environments with Raman and Luminescence for Organics and Chemicals (SHERLOC) investigation. Space Sci. Rev. **217**, 58 (2021). https://doi.org/10.1007/s11214-021-00812-z

L. Cameron, *Geocaching Handbook: The Guide for Family Friendly, High-Tech Treasure Hunting*, 3rd edn. (Falcon Guides, Guilford, 2017). ISBN 9781493027927

J.L. Campbell, P.L. King, L. Burkemper, J.A. Berger, R. Gellert, N.I. Boyd, G.M. Perrett, I. Pradler, L. Thompson, K.S. Edgett, R.A. Yingst, The Mars science laboratory APXS calibration target: comparison of Martian measurements with the terrestrial calibration. Nucl. Instrum. Methods Phys. Res., Sect. B, Beam Interact. Mater. Atoms **323**, 49–58 (2014). https://doi.org/10.1016/j.nimb.2014.01.011

B. Carrier, W.J. Abbey, L.W. Beegle, R. Bhartia, Y. Liu, Attenuation of ultraviolet radiation in rocks and minerals: implications for Mars science. J. Geophys. Res., Planets **124**(10), 2599–2612 (2019). https://doi.org/10.1029/2018JE005758

A. Cousin, P.Y. Meslin, R.C. Wiens, W. Rapin, N. Mangold, C. Fabre, O. Gasnault, O. Forni, R. Tokar, A. Ollila, S. Schröder, J. Lasue, S. Maurice, V. Sautter, H. Newsom, D. Vaniman, S. Le Mouélic, D. Dyar, G. Berger, D. Blaney, M. Nachon, G. Dromart, N. Lanza, B. Clark, S. Clegg, W. Goetz, J. Berger, B. Barraclough, D. Delapp (MSL Science Team), Compositions of coarse and fine particles in Martian soils at Gale: a window into the production of soils. Icarus **249**, 22–42 (2015). https://doi.org/10.1016/j.icarus.2014.04.052

A. Doyle, The adventure of the dancing men. The Strand (1903)

K.S. Edgett, Perseverance's SHERLOC WATSON – post-landing refinement of relations between focus, range, and image scale using images acquired on Mars, plus an update on particulates on the detector. https://doi.org/10.5281/zenodo.5555292. Zenodo (2021)

K.S. Edgett, M.A. Caplinger, J.N. Maki, M.A. Ravine, F.T. Ghaemi, S. McNair, K.E. Herkenhoff, B.M. Duston, R.G. Willson, R.A. Yingst, M.R. Kennedy, M.E. Minitti, A.J. Sengstacken, K.D. Supulver, L.J. Lipkaman, G.M. Krezoski, M.J. McBride, T.L. Jones, B.E. Nixon, J.K. Van Beek, D.J. Krysak, R.L. Kirk, Curiosity's robotic arm-mounted Mars Hand Lens Imager (MAHLI): Characterization and calibration status. MSL MAHLI Technical Report 0001 (2015). https://doi.org/10.13140/RG.2.1.3798.5447. Version 2, 05

K.A. Farley, K.H. Williford, K.M. Stack, R. Bhartia, A. Chen, M. de la Torre, K. Hand, Y. Goreva, C.D.K. Herd, R. Hueso, Y. Liu, J.N. Maki, G. Martinez, R.C. Moeller, A. Nelessen, C.E. Newman, D. Nunes, A. Ponce, N. Spanovich, P.A. Willis, L.W. Beegle, J.F. Bell III., A.J. Brown, S-E. Hamran, J.A. Hurowitz, S. Maurice, D.A. Paige, J.A. Rodriguez-Manfredi, M. Schulte, R.C. Wiens, Mars 2020 mission overview. Space Sci. Rev. **216**, 142 (2020). https://doi.org/10.1007/s11214-020-00762-y

T.G. Graff, R. Bhartia, L.W. Beegle, V.D. Tran, R.H. Weiner, M.J. Calaway, D.H. Garrison, M.D. Fries, K.N. Davis, A.S. Burton, A.J. Ross, C.L. Smith, The calibration target for the Mars 2020 SHERLOC instrument, in *50th Lunar and Planetary Science Conference 2019* (2019), p. 2132

L.B. Gram-Hansen, Geocaching in a persuasive perspective, in *Persuasive Technology, Fourth International Conference*, California, USA, April 26–29 (2009). https://doi.org/10.1145/1541948.1541993

J.D. Hein, D. Aldrich, E. Hochberg, A.C. Houck, E.A. Miller, R. Pollack, M.O. Shelton, R. Simon, V. Vorperian, W.F. Hug, R. Reid, L. DeFlores, L.W. Beegle, R. Bhartia, Test facilities for SHERLOC laser development, in *2022 IEEE Aerospace Conference* (2022)

J. Helbert, S. Del Togno, A. Maturilli, S. Ferrari, M. Grott, T. Okada, A novel spectral and radiometric calibration target for the TIR imager and the MARA instrument on the Hayabusa2 mission, in *45th Lunar and Planetary Science Conference* (2014), p. 1317

Internet Resource 1: geocaching trackable target on the SHERLOC calibration target (Accessed 14 February 2022). https://www.geocaching.com/track/details.aspx?id=4638861

Internet Resource 2: Meteoritical Society Database for SaU 008 meteorite (Accessed 21 October 2021). https://www.lpi.usra.edu/meteor/metbull.php?code=23200

JPL D-95514, JPL D-95514, Mars 2020 Project Contamination Control Implementation Plan (2020)

K.M. Kinch, M.B. Madsen, J.F. Bell III., J.N. Maki, Z. Bailey, A.G. Hayes, O.B. Jensen, M. Merusi, M.H. Bernt, A.N. Sørensen, M. Hilverda, E. Cloutis, D. Applin, E. Mateo-Marti, J.A. Manrique, G. Lopez-Reyes, A. Bello-Arufe, B.L. Ehlmann, J. Buz, A. Pommerol, N. Thomas, L. Affolter, K. Herkenhoff, J.R. Johnson, M. Rice, P. Corlies, C. Tate, M. Caplinger, E. Jensen, T. Kubacki, E. Cisneros, K. Paris, A. Winhold, Radiometric calibration targets for the Mastcam-Z camera on the Mars 2020 rover mission. Space Sci. Rev. (2020). https://doi.org/10.1007/s11214-020-00774-8

K. Larson, M.D. Fries, Ultraviolet testing of space suit materials for Mars, in *47th International Conference on Environmental Systems* (2017)

G. Lopez-Reyes, C. Pilorget, A.G. Moral, J.A. Manrique, A. Sanz, A. Berrocal, M. Veneranda, F. Rull, J. Medina, V. Hamm, J.P. Bibring, Raman Laser Spectrometer (RLS) calibration target design to allow onboard combined science between the RLS and MicrOmega instruments on the ExoMars rover. J. Raman Spectrosc. **51**(9), 1718–1730 (2020). https://doi.org/10.1002/jrs.5832

J.N. Maki, D. Gruel, C. McKinney, M.A. Ravine, M. Morales, D. Lee, R. Willson, D. Copley-Woods, M. Valvo, T. Goodsall, J. McGuire, R.G. Sellar, J.A. Schaffner, M.A. Caplinger, J.M. Shamah, A.E. Johnson, H. Ansari, K. Singh, T. Litwin, R. Deen, A. Culver, N. Ruoff, D. Petrizzo, D. Kessler, C. Basset, T. Estlin, F. Alibay, A. Nelessen, S. Algermissen, The Mars 2020 engineering cameras and microphone on the perseverance rover: a next-generation imaging system for Mars exploration. Space Sci. Rev. **216**, 137 (2020). https://doi.org/10.1007/s11214-020-00765-9

J.A. Manrique, G. Lopez-Reyes, A. Cousin, F. Rull, S. Maurice, R.C. Wiens, M.B. Madsen, J.M. Madariaga, O. Gasnault, J. Aramendia, G. Arana, SuperCam calibration targets: design and development. Space Sci. Rev. **216**(8), 1–27 (2020). https://doi.org/10.1007/s11214-020-00764-w

L. Matherson, V.H. Wright, C.T. Inman, E.K. Wilson, Get up, get out with geocaching: engaging technology for the social studies classroom Soc. Stud. Res. Pract. **3**(3), 80–85 (2008)

F.M. McCubbin, C.D.K. Herd, T. Yada, A. Hutzler, M.J. Calaway, J.H. Allton, C.M. Corrigan, M.D. Fries, A.D. Harrington, T.J. McCoy, J.L. Mitchell, A.B. Regberg, K. Righter, C.J. Snead, K.T. Tait, M.E. Zolensky, R.A. Zeigler, Advanced curation of astromaterials for planetary science. Space Sci. Rev. **215**, 48 (2019). https://doi.org/10.1007/s11214-019-0615-9

K. O'Hara, Understanding geocaching practices and motivations, in *Proceedings of the 2008 Conference on Human Factors in Computing Systems* (2008). https://doi.org/10.1145/1357054.1357239

J. Razzell Hollis, T. Fornaro, W. Rapin, J. Wade, A. Vicente-Retortillo, A. Steele, R. Bhartia, L.W. Beegle, Detection and degradation of adenosine monophosphate in perchlorate-spiked Martian regolith analogue, by deep-ultraviolet spectroscopy. Astrobiology **21**(5), 511–525 (2021a). https://doi.org/10.1089/ast.2020.2362

J. Razzell Hollis, W. Abbey, L.W. Beegle, R.Bhartia.B.E. Ehlmann, J. Miura, B. Monacelli, K. Moore, A. Nordman, E. Scheller, K. Uckert, Y-H. Wu, A deep-ultraviolet Raman and fluorescence spectral library of 62 minerals for the SHERLOC instrument onboard Mars 2020. Planet. Space Sci. **209**, 105356 (2021b). https://doi.org/10.1016/j.pss.2021.105356

B.E. Schlatter, A.R. Hurd, Geocaching: 21st century hide-and-seek. J. Phys. Educ. Recreat. Dance **67**(7), 28–32 (2005). https://doi.org/10.1080/07303084.2005.10609309

M.E. Schmidt, G.M. Perrett, S.L. Bray, N.J. Bradley, R.E. Lee, J.A. Berger, J.L. Campbell, C. Ly, S.W. Squyers, D. Tesselaar, Dusty rocks in Gale crater: assessing areal coverage and separating dust and rock contributions in APXS analyses. J. Geophys. Res., Planets **123**(7), 1649–1673 (2015). https://doi.org/10.1029/2018JE005553

E. Schudiske, The first geocaching first-to-find in space. Geocaching Official Blog, 18 November 2013. (Accessed 13 November 2021). https://www.geocaching.com/blog/2013/11/the-first-geocaching-first-to-find-in-space/

A. Steele, F.M. McCubbin, M. Fries, L. Kater, N.Z. Boctor, M.L. Fogel, P.G. Conrad, M. Glamoclija, M. Spencer, A.L. Morrow, M.R. Hammond, A reduced organic carbon component in Martian basalts. Science **337**(6091), 212–215 (2012). https://doi.org/10.1126/science.1220715

A. Steele, F.M. McCubbin, M.D. Fries, The provenance, formation, and implications of reduced carbon phases in Martian meteorites. Meteorit. Planet. Sci. **51**(11), 2203–2225 (2016). https://doi.org/10.1111/maps.12670

A. Steele, L.G. Benning, R. Wirth, S. Siljeström, M.D. Fries, E. Hauri, P.G. Conrad, K. Rogers, J. Eigenbrode, A. Schreiber, A. Needham, Organic synthesis on Mars by electrochemical reduction of CO_2. Sci. Adv. **4**(10), 1–10 (2018). https://doi.org/10.1126/sciadv.aat5118

A. Steele, L.G. Benning, R. Wirth, A. Schreiber, T. Araki, F.M. McCubbin, M.D. Fries, L.R. Nittler, J. Wang, L.J. Hallis, P.G. Conrad, C. Conley, S. Vitale, A.C. O'Brien, V. Riggi, K. Rogers, Organic synthesis associated with serpentinization and carbonation on early Mars. Science **375**(6577), 172–177 (2022). https://doi.org/10.1126/science.abg7905

K. Uckert, R. Bhartia, L.W. Beegle, B. Monacelli, S.A. Asher, A.S. Burton, S. Bykov, K. Davis, M.D. Fries, R.S. Jakubek, J. Razzell Hollis, R.D. Roppel, Y-H. Wu, Calibration of the SHERLOC deep ultraviolet fluorescence-Raman spectrometer on the perseverance rover. Appl. Spectrosc. **75**(7), 763–773 (2021). https://doi.org/10.1177/00037028211013368

B.V. Wogsland et al., SHERLOC and WATSON imaging with the perseverance rover: science and science enabling activities. J. Geophys. Res., Planets (2022, submitted)

E. Worthy, Process specification for cleaning of hardware (2020). Engineering Directorate, Structural Engineering Division, NASA Johnson Space Center, PRC-5001, Rev. G. https://mmptdpublic.jsc.nasa.gov/prc/PRC-5001_Current.pdf

R.A. Yingst, K.S. Edgett, M.R. Kennedy, G.M. Krezoski, M.J. McBride, M.E. Minitti, M.A. Ravine, R.M.E. Williams, MAHLI on Mars: lessons learned operating a geoscience camera on a landed payload robotic arm. Geosci. Instrum. Method. Data Syst. **5**, 205–217 (2016). https://doi.org/10.5194/gi-5-205-2016

R.A. Yingst, S. Bray, K. Herkenhoff, M. Lemmon, M.E. Minitti, M.E. Schmidt, K.S. Edgett, D.M. Fey, L.C. Kah, Dust cover on curiosity's Mars Hand Lens Imager (MAHLI) calibration target: implications for deposition and removal mechanisms. Icarus **351**, 113872 (2020). https://doi.org/10.1016/j.icarus.2020.113872

S. Zecha, L. Hilger, EarthCaches: an opportunity for learning geoscience; a pilot study for glaciomorphologically themes EarthCaches. Int. J. Geogr. Inf. Sci. **3**, 324–334 (2015). https://doi.org/10.1553/giscience2015s324

S. Zecha, A. Regelous, Promoting geodiversity education by using EarthCaching in national geoparks. Geoheritage **10**, 637–643 (2018). https://doi.org/10.1007/s12371-018-0280-5

Authors and Affiliations

Marc D. Fries[1] · Carina Lee[2] · Rohit Bhartia[3] · Joseph Razzell Hollis[4] · Luther W. Beegle[5] · Kyle Uckert[5] · Trevor G. Graff[6] · William Abbey[5] · Zachary Bailey[5] · Eve L. Berger[7] · Aaron S. Burton[1] · Michael J. Callaway[6] · Emily L. Cardarelli[5] · Kristine N. Davis[1] · Lauren DeFlores[5] · Kenneth S. Edgett[8] · Allison C. Fox[9] · Daniel H. Garrison[6] · Nikole C. Haney[6] · Roger S. Harrington[6] · Ryan S. Jakubek[6] · Megan R. Kennedy[8] · Keyron Hickman-Lewis[4] · Francis M. McCubbin[1] · Ed Miller[5] · Brian Monacelli[5] · Randy Pollock[5] · Richard Rhodes[6] · Sandra Siljeström[10] · Sunanda Sharma[5] · Caroline L. Smith[4] · Andrew Steele[11] · Margarite Sylvia[5] · Vinh D. Tran[6] · Ryan H. Weiner[6] · Anastasia G. Yanchilina[12] · R. Aileen Yingst[13]

✉ W. Abbey
william.j.abbey@jpl.nasa.gov

1   NASA Johnson Space Center, 77058 Houston, TX, USA

2   Lunar and Planetary Institute, Universities Space Research Association, Houston, TX, USA

3   Photon Systems Inc., 1512 Industrial Park St., 91722 Covina, CA, USA

[4] Natural History Museum, London, UK

[5] Jet Propulsion Laboratory, California Institution of Technology, 4800 Oak Grove Drive, 91109 Pasadena, CA, USA

[6] Jacobs JETS, NASA Johnson Space Center, 77058 Houston, TX, USA

[7] Jacobs JETS, NASA Johnson Space Center, Texas State University, 77058 Houston, TX, USA

[8] Malin Space Science Systems, Inc., San Diego, CA, USA

[9] NASA Johnson Space Center, NASA Postdoctoral Program, 77058 Houston, TX, USA

[10] RISE Research Institutes of Sweden, 11486 Stockholm, Sweden

[11] Carnegie Institute of Washington, Washington, DC, USA

[12] Impossible Sensing, St. Louis, MO, USA

[13] Planetary Science Institute, Tucson, AZ, USA